

SINDy-PI: A Robust Algorithm for Parallel Implicit Sparse Identification of Nonlinear Dynamics

Kadierdan Kaheman^{1*}, J. Nathan Kutz², Steven L. Brunton¹

¹ Department of Mechanical Engineering, University of Washington, Seattle, WA 98195, United States

² Department of Applied Mathematics, University of Washington, Seattle, WA 98195, United States

Abstract

Accurately modeling the nonlinear dynamics of a system from measurement data is a challenging yet vital topic. The sparse identification of nonlinear dynamics (SINDy) algorithm is one approach to discover dynamical systems models from data. Although extensions have been developed to identify implicit dynamics, or dynamics described by rational functions, these extensions are extremely sensitive to noise. In this work, we develop SINDy-PI (parallel, implicit), a robust variant of the SINDy algorithm to identify implicit dynamics and rational nonlinearities. The SINDy-PI framework includes multiple optimization algorithms and a principled approach to model selection. We demonstrate the ability of this algorithm to learn implicit ordinary and partial differential equations and conservation laws from limited and noisy data. In particular, we show that the proposed approach is several orders of magnitude more noise robust than previous approaches, and may be used to identify a class of ODE and PDE dynamics that were previously unattainable with SINDy, including for the double pendulum dynamics and simplified model for the Belousov–Zhabotinsky (BZ) reaction.

1 Introduction

Discovering dynamical system models from data is critically important across science and engineering. Traditionally, models are derived from first principles, although this approach may be prohibitively challenging in many fields, such as climate science, finance, and biology. Fortunately, data-driven model discovery (i.e., system identification) is a rapidly developing field [1], with a range of techniques including classic linear approaches [2, 3], dynamic mode decomposition (DMD) [4, 5] and Koopman theory [6–9], nonlinear autoregressive models [10, 11], neural networks [12–20], Gaussian process regression [21, 22], nonlinear Laplacian spectral analysis [23], diffusion maps [24], genetic programming [25–27], and sparse regression [28–30], to highlight some of the recent developments. Of particular note is a recent push towards *parsimonious* modeling [25, 26, 28], which favors Pareto-optimal models with the lowest complexity required to describe the observed data. These models benefit from being interpretable, and they tend to generalize and prevent overfitting. The sparse identification of nonlinear dynamics (SINDy) algorithm [28] discovers parsimonious models through a sparsity-promoting optimization to select only a few model terms from a library of candidate functions. SINDy has been widely adopted in the community [30–46], but it relies on the dynamics having a sparse representation in a pre-defined library, making it difficult to discover implicit dynamics and rational functions. The implicit-SINDy extension [47] makes it possible to identify these implicit functions, although this algorithm is extremely sensitive to noise. In this work, we develop a robust, parallel algorithm for the sparse identification of implicit dynamics, making it possible to explore entirely new classes of systems that were previously inaccessible.

* Corresponding author (kadierk@uw.edu); Code availalbe at github.com/dynamicslab/SINDy-PI.

Parsimonious modeling has a rich history, with many scientific advances being argued on the basis of Occam's razor, that the simplest model is likely the correct one. SINDy exemplifies this principle, identifying a potentially nonlinear model with the fewest terms required to describe how the measurement data changes in time. The basic idea behind SINDy may be illustrated on a one-dimensional system $\dot{x} = f(x)$; the general formulation for multidimensional dynamics will be described in the following sections. An interpretable form of the nonlinear dynamics may be learned by writing the rate of change of the state of the system x as a sparse linear combination of a few terms in a library of candidate functions, $\Theta(x) = [\theta_1(x) \quad \theta_2(x) \quad \dots \quad \theta_p(x)]$:

$$\dot{x}(t) = f(x(t)) \approx \Theta(x(t))\xi. \quad (1)$$

where each $\theta_j(x)$ is prescribed candidate term (e.g. $x, x^2, \sin(x), \dots$). The derivative of the state and the library of candidate functions may both be computed from measured trajectory data. It then remains to solve for a sparse vector ξ with nonzero entries ξ_j indicating which functions $\theta_j(x)$ are active in characterizing the dynamics. The resulting models strike a balance between accuracy and efficiency, and they are highly interpretable by construction. In a short time, the SINDy algorithm has been extended to include inputs and control [48], to identify partial differential equations [29, 30], to incorporate physically relevant constraints [34], to include tensor bases [45], and to incorporate integral terms for denoising [49, 50]. These extensions and its simple formulation in terms of a generalized linear model in (1) have resulted in SINDy being adopted in the fields of fluid mechanics [34, 37], nonlinear optics [31], plasma physics [32], chemical reactions [33, 36, 39], numerical methods [41], and structural modeling [42].

The generalized linear model in (1) does not readily lend itself to representing implicit dynamics and rational functions, which are not naturally expressible as sum of a few basis functions. Instead, the implicit-SINDy algorithm [47] reformulates the SINDy problem in an implicit form:

$$\Theta(x, \dot{x})\xi = 0. \quad (2)$$

This formulation is flexible enough to handle a much broader class of dynamics with rational function nonlinearities, such as $\dot{x} = N(x)/D(x)$ which may be rewritten as $\dot{x}D(x) + N(x) = 0$. However, the sparsest vector ξ that satisfies (2) is the trivial solution $\xi = 0$. Thus, the implicit-SINDy algorithm leverages a recent non-convex optimization procedure [51, 52] to find the sparsest vector ξ in the null space of $\Theta(x, \dot{x})$, which differs from other approaches [53, 54] that identify the rational dynamics. For even small amounts of noise, the dimension of the null space will become prohibitively large, making this approach extremely sensitive to noise and compromising the model discovery process.

This work develops an optimization and model selection framework that recasts implicit-SINDy as a convex problem, making it as noise robust as the original non-implicit SINDy algorithm and enabling the identification of implicit ODEs and PDEs that were previously inaccessible. The key to making the implicit-SINDy algorithm robust is the realization that if we know even a single term in the dynamics, corresponding to a non-zero entry ξ_j , then we can rewrite (2) in a non-implicit form

$$\theta_j(x, \dot{x}) = \Theta'(x, \dot{x})\xi' \quad (3)$$

where Θ' and ξ' have the j -th element removed. Because none of these terms are known *a priori*, we sweep through the library, term by term, testing (3) for a sparse model that fits the data. This procedure is highly parallelizable and provides critical information for model selection. Our approach is related to the recent work of Zhang et al. [46], which also makes the implicit problem more robust by testing candidate functions individually. However, there are a number of key

differences in the present approach. Our work explicitly considers *rational* nonlinearities to discover exceedingly complex implicit PDEs, such as a simplified model of the Belousov-Zhabotinsky (BZ) reaction. Our framework also provides several new greedy algorithms, including parallel and constrained formulations. We further extend this method to include the effect of control inputs, making it applicable to robotic systems [55], and we use this procedure to discover Hamiltonians. Finally, our approach provides guidance on model selection, a comprehensive comparison with previous methods, and a careful analysis of noise robustness.

2 Background

We briefly introduce the full multidimensional SINDy and implicit-SINDy algorithms, which will provide a foundation for our robust implicit identification algorithm in Sec. 3.

2.1 Sparse Identification of Nonlinear Dynamics

The goal of SINDy [28] is to discover a dynamical system

$$\frac{d}{dt} \mathbf{x}(t) = \mathbf{f}(\mathbf{x}(t)), \quad (4)$$

from time-series data of the state $\mathbf{x}(t) = [x_1(t), \dots, x_n(t)]^T \in \mathbb{R}^n$. We assume that the dynamics, encoded by the function \mathbf{f} , admit a sparse representation in a library of candidate functions:

$$\Theta(\mathbf{x}) = [\theta_1(\mathbf{x}) \quad \theta_2(\mathbf{x}) \quad \dots \quad \theta_p(\mathbf{x})]. \quad (5)$$

Thus, each row equation in (4) may be written as

$$\frac{d}{dt} x_k(t) = f_k(\mathbf{x}(t)) \approx \Theta(\mathbf{x}) \xi_k \quad (6)$$

where ξ_k is a sparse vector, indicating which terms are active in the dynamics.

We determine the nonzero entries of ξ_k through sparse regression based on trajectory data. The time-series data is arranged into a matrix $\mathbf{X} = [\mathbf{x}(t_1) \quad \mathbf{x}(t_2) \quad \dots \quad \mathbf{x}(t_m)]^T$, and the associated time derivative matrix $\dot{\mathbf{X}} = [\dot{\mathbf{x}}(t_1) \quad \dot{\mathbf{x}}(t_2) \quad \dots \quad \dot{\mathbf{x}}(t_m)]^T$ is computed using an appropriate numerical differentiation scheme [1, 28, 56]. It is then possible to evaluate the library Θ on trajectory data in \mathbf{X} so that each column of $\Theta(\mathbf{X})$ is a function θ_j evaluated on the m snapshots in \mathbf{X} .

It is now possible to write the dynamical system in terms of a generalized linear model, evaluated on trajectory data:

$$\dot{\mathbf{X}} = \Theta(\mathbf{X}) \Xi. \quad (7)$$

There are several approaches to identify the sparse matrix of coefficients Ξ , including sequentially thresholded least squares (STLSQ) [28, 57], LASSO [58], sparse relaxed regularized regression (SR3) [59, 60], stepwise sparse regression (SSR) [36], and Bayesian approaches [46, 61]. It is possible to augment the library to include partial derivatives for the identification of partial differential equations (PDEs) [29, 30]. Similarly, it is possible to include external forcing terms in the library Θ , enabling the identification of forced and actively controlled systems [48]. To alleviate the effect of noise, it is possible to reframe the SINDy problem in terms of an integral formulation [49, 50]. There are a number of factors that affect the robustness of SINDy, some of which are discussed in App. I.

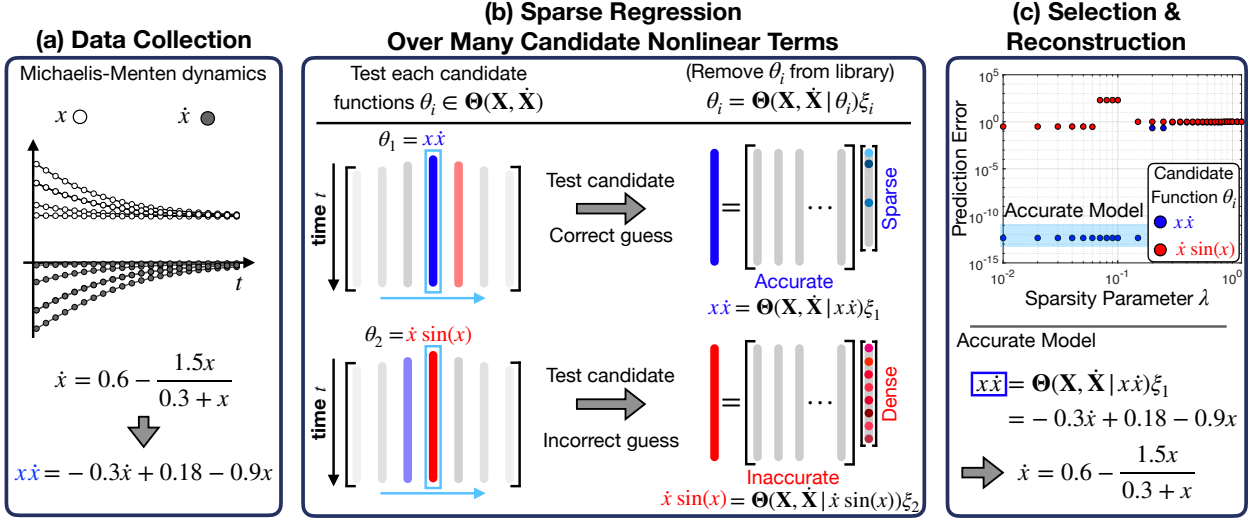


Figure 1: The illustration of the SINDy-PI algorithm on Michaelis-Menten dynamics. (a) The Michaelis-Menten system is simulated, and measurement data is provided to SINDy-PI. (b) Multiple possible left-hand side functions are tested at the same time. (c) The candidate model prediction error is calculated, and the best model is selected.

2.2 Implicit Sparse Identification of Nonlinear Dynamics

The implicit-SINDy algorithm [47] extends SINDy to identify implicit differential equations

$$\mathbf{f}(\mathbf{x}, \dot{\mathbf{x}}) = 0, \quad (8)$$

and in particular, systems that include rational functions in the dynamics, such as chemical reactions and metabolic networks that have a separation of timescales.

The implicit-SINDy generalizes the library $\Theta(\mathbf{X})$ in (7) to include functions of \mathbf{x} and $\dot{\mathbf{x}}$:

$$\Theta(\mathbf{X}, \dot{\mathbf{X}})\Xi = 0. \quad (9)$$

However, this approach requires solving for a matrix Ξ whose columns ξ_k are sparse vectors in the null space of $\Theta(\mathbf{X}, \dot{\mathbf{X}})$. This approach is non-convex, relying on the alternating directions method (ADM) [47, 52], and null space computations are highly ill-conditioned for noisy data [1, 47, 62], thus inspiring the current work and mathematical innovations.

3 SINDy-PI: Robust Parallel Identification of Implicit Dynamics

We have developed the SINDy-PI (parallel, implicit) framework for the robust identification of implicit dynamics, bypassing the null space approach discussed in Sec. 2.2. The idea is that if even a single term $\theta_j(\mathbf{x}, \dot{\mathbf{x}}) \in \Theta(\mathbf{x}, \dot{\mathbf{x}})$ in the dynamics (8) is known, it is possible to rewrite (9) as

$$\theta_j(\mathbf{X}, \dot{\mathbf{X}}) = \Theta(\mathbf{X}, \dot{\mathbf{X}}|\theta_j(\mathbf{X}, \dot{\mathbf{X}})\xi_j), \quad (10)$$

where $\Theta(\mathbf{X}, \dot{\mathbf{X}}|\theta_j(\mathbf{X}, \dot{\mathbf{X}}))$ is the library $\Theta(\mathbf{X}, \dot{\mathbf{X}})$ with the θ_j column removed. Equation (10) is no longer in implicit form, and the sparse coefficient matrix corresponding to the remaining terms may be solved for using previously developed SINDy techniques [28–30, 36, 46, 49, 50, 59–61]. In particular, we solve for a sparse coefficient vector ξ_j that minimizes the following loss function:

$$\|\theta_j(\mathbf{X}, \dot{\mathbf{X}}) - \Theta(\mathbf{X}, \dot{\mathbf{X}}|\theta_j(\mathbf{X}, \dot{\mathbf{X}})\xi_j)\|_2 + \beta \|\xi_j\|_0, \quad (11)$$

where β is the sparsity promoting parameter. There are numerous relaxations of the non-convex optimization problem in (11), for example the sequentially thresholded least-squares algorithm [28]. Because there is no null space calculation, the resulting algorithm is considerably more robust to noise than the implicit-SINDy algorithm [47], i.e. we longer have to deal with an ill-conditioned null space problem.

In general, the entire point of SINDy is that the dynamics are not known ahead of time, and so it is necessary to test each candidate function θ_j until one of the models in (10) admits a sparse and accurate solution. When an incorrect candidate term is used, then the algorithm results in a dense (non-sparse) model ξ_j and an inaccurate model fit, and when a correct term is included, the algorithm identifies a sparse model ξ_j and an accurate model fit. In this way, it is clear when the algorithm has identified the correct model. Moreover, there is a wealth of redundant information, since each term in the correct model may be used as the candidate function on the left hand side, and the resulting models may be cross-referenced. This approach is highly parallelizable, and each candidate term may be tested simultaneously in parallel. The non-parallel formulation in (10) was recently introduced by Zhang et al. [46] in the context of Bayesian regression, where they also make the implicit problem more robust by testing candidate functions individually; however, they do not consider dynamics with rational function nonlinearities or control inputs. In this work, we extend the robust implicit formulation to identify several challenging implicit ODE and PDE systems with rational function nonlinearities, which are ubiquitous in engineering and natural systems, and systems with external forcing and control inputs. We also introduce the parallel formulation and model selection frameworks. Further, we will introduce a constrained optimization framework to simultaneously test all candidate functions.

3.1 Model Selection

For each candidate function in (10), we obtain one candidate model. When the candidate function θ_j is not in the true dynamics, then the resulting coefficient vector ξ_j will not be sparse and there will be large prediction error. In contrast, when a correct candidate function is selected, then we obtain a sparse coefficient vector ξ_j and small prediction error. For an implicit dynamical system, there may be several different implicit equations that must be identified, resulting in several candidate functions that admit sparse models. The sequentially thresholded least squares (STLSQ) algorithm that we use here, and whose convergence properties are considered by Zhang and Schaeffer [57], iteratively computes a least-squares solution to minimize $\|\theta_j(\mathbf{X}, \dot{\mathbf{X}}) - \Theta(\mathbf{X}, \dot{\mathbf{X}}|\theta_j(\mathbf{X}, \dot{\mathbf{X}}))\xi_j\|_2$ and then zeros out small entries in ξ_j that are below a set threshold λ . This threshold λ is a hyperparameter that must be tuned to select the model that most accurately balances accuracy and efficiency. Thus, we must employ model selection techniques to identify the implicit models that best supports the data, while remaining as simple as possible.

There are several valid approaches to model selection. To select a parsimonious yet accurate model we can also employ the Akaike information criterion (AIC) [63, 64] and Bayesian information criterion (BIC) [65], as in [66]. It is also possible to sweep through the parameter λ and candidate functions θ_j , and then choose the Pareto optimal model from a *family* of models on the Pareto front balancing accuracy and efficiency; this is the approach in the original SINDy work [28] and in earlier work leveraging genetic programming to discover dynamics [25, 26]. In this work, we take a different approach, selecting models based on performance on a test data set \mathbf{X}_t that has been withheld for model validation to automate the model selection process. For each threshold λ , the resulting model is validated on the test set \mathbf{X}_t , and the model with the lowest test error is selected.

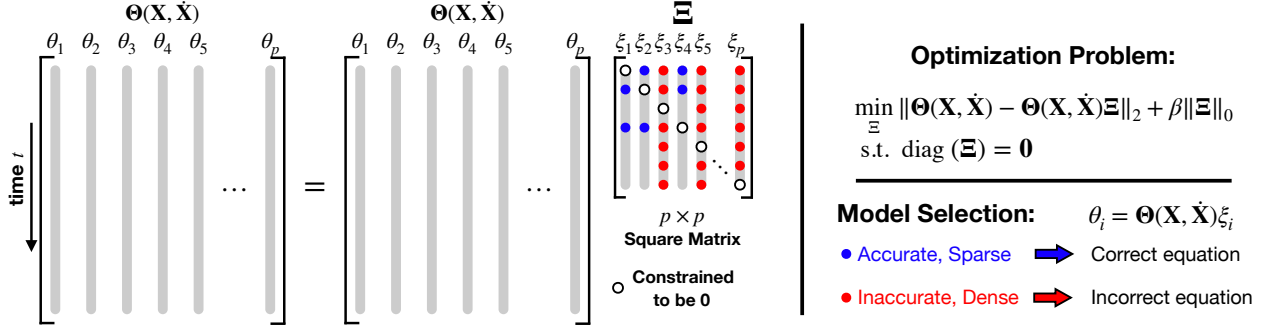


Figure 2: Schematic illustrating the constrained formulation of the SINDy-PI algorithm.

One error function is the model fit:

$$\text{Error} = \frac{\|\theta_j(\mathbf{X}_t, \dot{\mathbf{X}}_t) - \Theta(\mathbf{X}_t, \dot{\mathbf{X}}_t | \theta_j(\mathbf{X}_t, \dot{\mathbf{X}}_t))\Xi\|_2}{\|\theta_j(\mathbf{X}_t, \dot{\mathbf{X}}_t)\|_2}. \quad (12)$$

In practice, for rational dynamics, we select based upon the predicted derivative $\dot{\mathbf{X}}_t$:

$$\text{Error} = \frac{\|\dot{\mathbf{X}}_t - \dot{\mathbf{X}}_t^{\text{model}}\|_2}{\|\dot{\mathbf{X}}_t\|_2}. \quad (13)$$

For implicit dynamics where each state derivative may be written as a rational function

$$\dot{x}_k = f_k(\mathbf{x}) = \frac{N_k(\mathbf{x})}{D_k(\mathbf{x})}, \quad (14)$$

then we restrict the candidate functions to $\theta_j(\mathbf{x}, \dot{\mathbf{x}}) = \dot{x}_k \theta_j(\mathbf{x})$ for some $\theta_j(\mathbf{x}) \in \Theta(\mathbf{x})$ to identify a separate sparse model for each \dot{x}_k . Several candidate functions may provide accurate and sparse models. These different models may further be cross-references to check that the same terms are being selected in each model, providing additional information for model selection and validation.

3.2 Constrained Optimization Formulation

In (10) each candidate function was tested individually in a parallel optimization. However, each of these individual equations may be combined into a single constrained system of equations

$$\Theta(\mathbf{X}, \dot{\mathbf{X}}) = \Theta(\mathbf{X}, \dot{\mathbf{X}})\Xi \quad \text{such that} \quad \Xi_{jj} = 0. \quad (15)$$

We constrain Ξ to have zero entries on the diagonal, as shown in Fig. 2, which is the same as removing the candidate function from the library in the separate optimization problems in (10). Without this constraint, the trivial solution $\Xi = \mathbb{I}_{p \times p}$ will provide the sparsest Ξ and the most accurate model. This may be written as a formal constrained optimization problem:

$$\begin{aligned} \min_{\Xi} \quad & \|\Theta(\mathbf{X}, \dot{\mathbf{X}}) - \Theta(\mathbf{X}, \dot{\mathbf{X}})\Xi\|_2 + \beta\|\Xi\|_0, \\ \text{s.t.} \quad & \text{diag}(\Xi) = \mathbf{0}. \end{aligned} \quad (16)$$

This optimization is non-convex, although there are many relaxations that result in accurate and efficient proxy solutions [28, 58, 59]. In this work, we will use sequentially thresholded least squares,

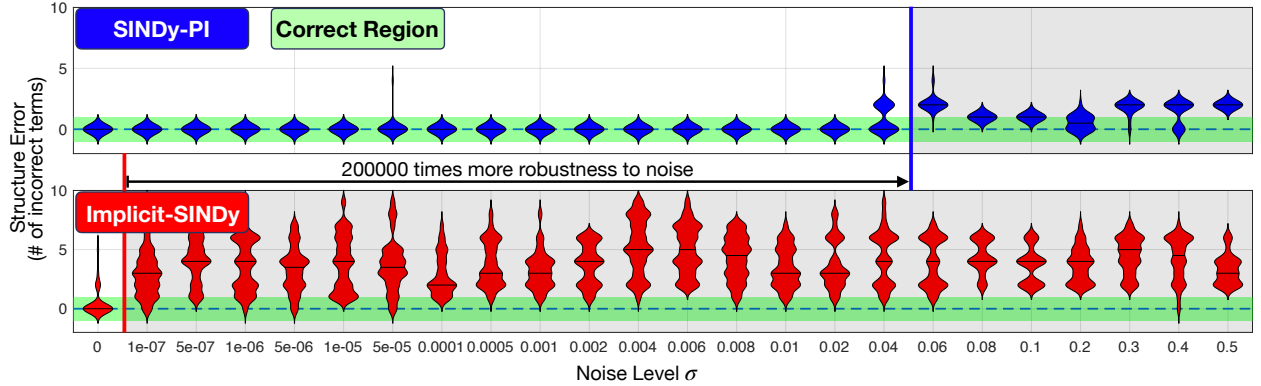


Figure 3: SINDy-PI and implicit-SINDy are compared on the Michaelis-Menten kinetics, where the structure error quantifies the number of terms in the model that are incorrectly added or deleted, compared with the true model. The derivative is computed by the total-variation regularization difference (TVRegDiff) [56] on noisy state measurements. The violin plots show the cross-validated distribution of the number of incorrect terms across 30 models. The green region indicates no structural difference between the identified model and the ground truth model. Details are provided in Appendix A.2.

so that any entry $\Xi_{ij} < \lambda$ will be set to zero; the sparsity parameter λ is a hyperparameter, and each column equation may require a different parameter λ_j . The constrained formulation in (16) can be solved efficiently in modern optimization packages, and we use CVX [67, 68]. After solving (16) we have numerous candidate models, one for each column ξ_k of Ξ , given by

$$\Theta(\mathbf{X}, \dot{\mathbf{X}})\xi_j = 0. \quad (17)$$

The sparse models that result in an accurate fit are candidate implicit models, and they may be assessed using the model selection approaches outlined above. These various models may be cross-referenced for consistency, as the same models will have the same sparsity pattern. This information can then be used to refine the library Θ , for example to only include the nonzero entries in the sparse columns of Ξ .

3.3 Noise Robustness

We now compare the noise sensitivity of SINDy-PI and implicit-SINDy on the one-dimensional Michaelis–Menten model for enzyme kinetics [47, 69, 70], given by

$$\dot{x} = j_x - \frac{V_{\max}x}{K_m + x}, \quad (18)$$

where x denotes the concentration of the substrate, j_x denotes the influx of the substrate, V_{\max} denotes the maximum reaction rate, and K_m represents the concentration of half-maximal reaction. We use the same parameters as in [47], with $j_x = 0.6$, $V_{\max} = 1.5$, and $K_m = 0.3$. Figure 3 shows the result of the noise robustness of SINDy-PI and implicit-SINDy. In this example, SINDy-PI is able to handle over 10^5 more measurement noise than implicit-SINDy, while still accurately recovering the correct model. Details are provided in App. A, and key factors that limit robustness are discussed in App. I.

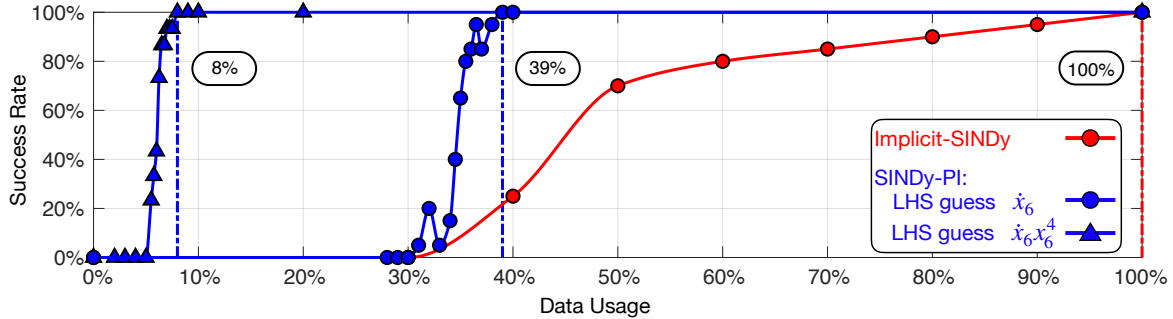


Figure 4: Success rate of SINDy-PI and implicit-SINDy identifying yeast glycolysis (19f) with different percentage of training data. Each data usage percentage is randomly sampled from the entire data set composed of all trajectories. The success rate is calculated by averaging the results of 20 runs.

3.4 Data Usage

The data required to correctly identify a model is a critical aspect when comparing SINDy-PI and implicit-SINDy. Many experimental data sets are limited in volume, and thus our goal is to identify a model with as little data as possible. In this section, we compare the SINDy-PI and implicit-SINDy methods on the challenging yeast glycolysis model [47, 71] given by

$$\dot{x}_1 = c_1 + \frac{c_2 x_1 x_6}{1 + c_3 x_6^4}, \quad (19a)$$

$$\dot{x}_2 = \frac{d_1 x_1 x_6}{1 + d_2 x_6^4} + d_3 x_2 - d_4 x_2 x_7, \quad (19b)$$

$$\dot{x}_3 = e_1 x_2 + e_2 x_3 + e_3 x_2 x_7 + e_4 x_3 x_6 + f_5 x_4 x_7, \quad (19c)$$

$$\dot{x}_4 = f_1 x_3 + e_2 x_4 + f_3 x_5 + f_4 x_3 x_6 + f_5 x_4 x_7, \quad (19d)$$

$$\dot{x}_5 = g_1 x_1 + g_2 x_5, \quad (19e)$$

$$\dot{x}_6 = h_3 x_3 + h_5 x_6 + h_4 x_3 x_6 + \frac{h_1 x_1 x_6}{1 + h_2 x_6^4}, \quad (19f)$$

$$\dot{x}_7 = j_1 x_2 + j_2 x_2 x_7 + j_3 x_4 x_7. \quad (19g)$$

Equation (19f) is the most challenging equation to discover in this system, and Fig. 4 compares the success rate of SINDy-PI and implicit-SINDy in identifying this equation. SINDy-PI uses about 12 times less data than the implicit-SINDy when identifying (19f). Details are provided in Appendices B and D.

3.5 Comparison for Implicit PDE Identification

We now investigate the ability of SINDy-PI to discover a PDE with rational terms, given by a modified KdV equation

$$u_t = -u_{xxx} - 6uu_x - \gamma u + \frac{2g_0}{1+u}, \quad (20)$$

where γu is a loss term and $2g_0/(1+u)$ is a gain term. We fix $\gamma = 0.1$ and vary the value of g_0 from 0 to 1. As g_0 increases, the implicit term gradually dominates the dynamics. Figure 5 shows the results of SINDy-PI and PDE-FIND [29] for different values of g_0 . For large g_0 , SINDy-PI is able to accurately identify the rational function term, while this is not possible for PDE-FIND, since this term is not in the library. Details of the identification process are given in App. C.

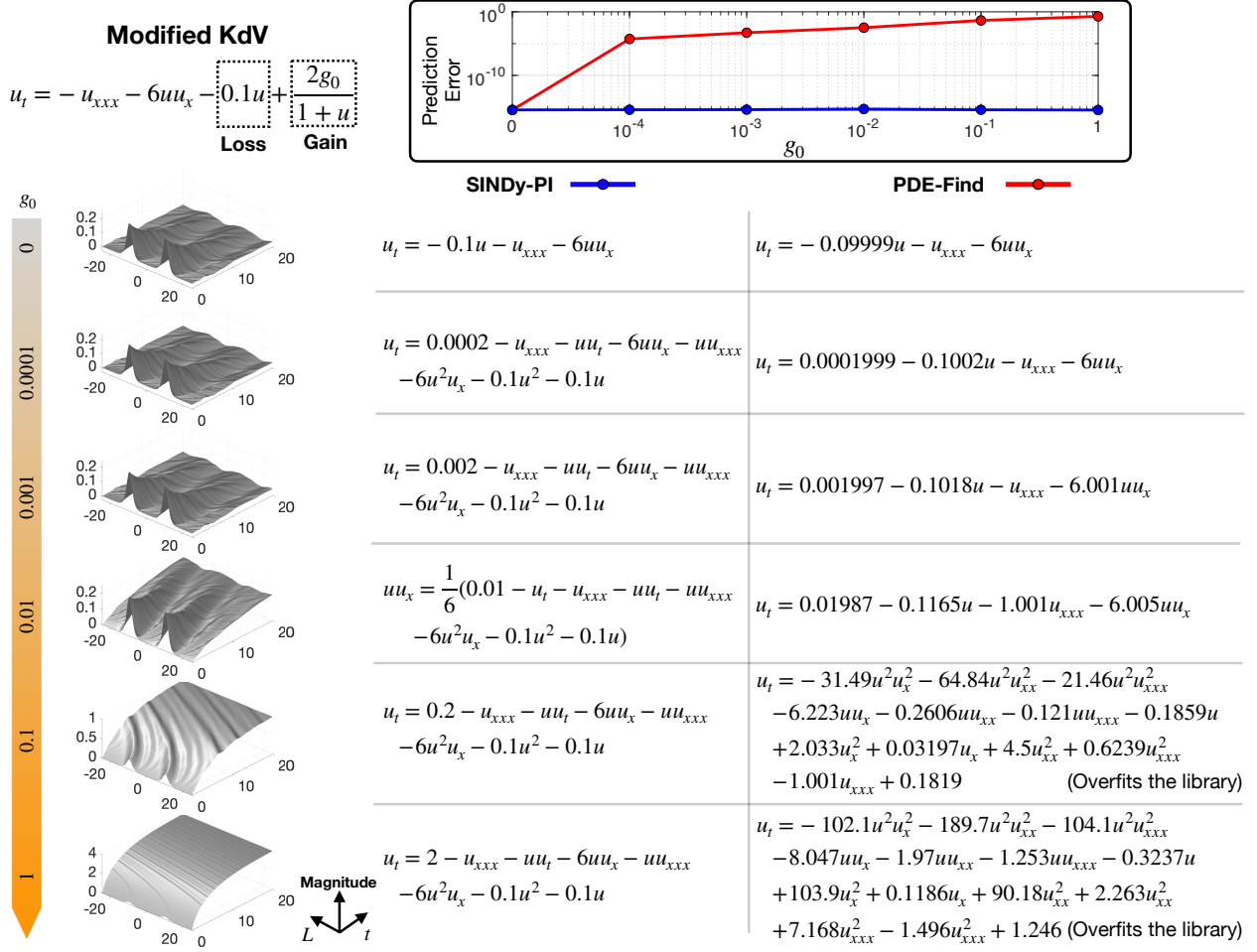


Figure 5: Comparison of SINDy-PI and PDE-FIND on an implicit PDE problem given by the modified KdV equation (20). As we increase g_0 , the rational term begins to play a significant role in the system behavior. For small g_0 , PDE-FIND compensates for the effect of the rational term by tuning the other coefficients. When g_0 is large, PDE-FIND overfits the library. SINDy-PI, on the other hand, correctly identifies the rational term.

4 Advanced Examples

We will now demonstrate the SINDy-PI framework on several challenging examples, including the double pendulum, an actuated single pendulum on a cart, the Belousov-Zhabotinsky PDE, and the identification of conserved quantities. All examples are characterized by rational nonlinearities, and we were unable to identify them using SINDy or implicit-SINDy, even in the absence of noise.

4.1 Mounted Double Pendulum

In our first example, we use SINDy-PI to discover the equations of motion of a mounted double pendulum, shown in Fig. 6. The double pendulum is a classic example of chaotic dynamics [72], and was an original challenging example used to demonstrate the capabilities of genetic program for model discovery [26]. Correctly modeling the nonlinear dynamics is vital for accurate control [72].

We simulate the double pendulum dynamics, derived from the Euler-Lagrange equations, and

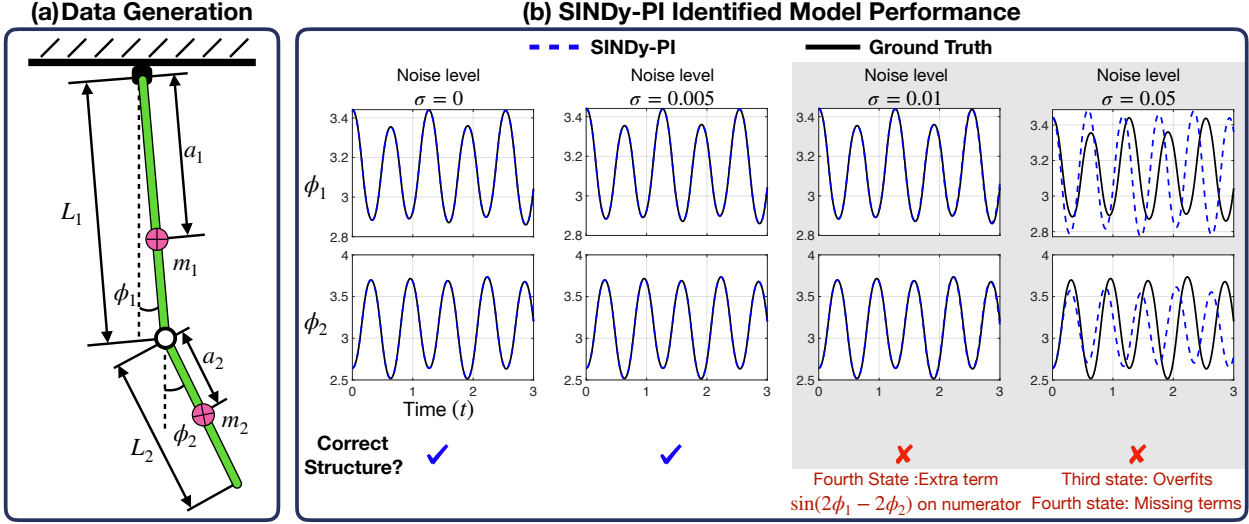


Figure 6: Schematic illustration of SINDy-PI identifying a mounted double pendulum system.

use SINDy-PI to re-discover the dynamics from noisy measurements of the trajectory data. The governing equations and SINDy-PI models are provided in App. F. Because these dynamics have rational nonlinearities, the original SINDy algorithm is unable to identify the dynamics, making this a challenging test case. The state vector is given by $\mathbf{x} = [\phi_1, \phi_2, \dot{\phi}_1, \dot{\phi}_2]^T$, and the parameters of the simulation are given in App. D. The training data is generated from an initial condition $x_{\text{train}} = [\pi + 1.2, \pi - 0.6, 0, 0]^T$, simulated for 10 seconds using a time step of $dt = 0.001$ seconds. The validation data is generated from an initial condition $x_{\text{val}} = [\pi - 1, \pi - 0.4, 0.3, 0.4]^T$, simulated for 3 seconds with time step $dt = 0.001$ seconds.

To test the robustness of SINDy-PI, we add Gaussian noise to both the training and validation data. We test the resulting models using a new testing initial condition $x_{\text{test}} = [\pi + 0.3, \pi - 0.5, 0, 0]^T$. We construct our library Θ to include over 40 trigonometric and polynomial terms. The most challenging part of this example is building a library with the necessary terms, without it growing too large. The library cannot be too extensive, or else the matrix Θ becomes ill conditioned, making it sensitive to noise. To reduce the library size, we use one piece of expert knowledge: the trigonometric terms should only consist of ϕ_1 and ϕ_2 , the rotational angles of the pendula.

The candidate functions are chosen as a combination of state derivatives and trigonometric functions. Fig. 6 shows that SINDy-PI can identify the equations of motion for low noise. For larger noise, SINDy-PI misidentifies the dynamics, although it still has short term prediction ability.

4.2 Single Pendulum on a Cart

We now apply SINDy-PI to identify a fractional ODE problem with control input, given by the single pendulum on a cart in Fig. 7. SINDy has already been extended to include control inputs [48], although the original formulation doesn't accommodate rational functions.

The dynamics are derived from the Euler-Lagrange equations. All system parameters except for gravity are chosen to be 1, as summarized in App. D; the governing equations and SINDy-PI models are shown in App. E. The cart position is denoted by s . The state vector is given by $\mathbf{x} = [\phi, s, \dot{\phi}, \dot{s}]^T$.

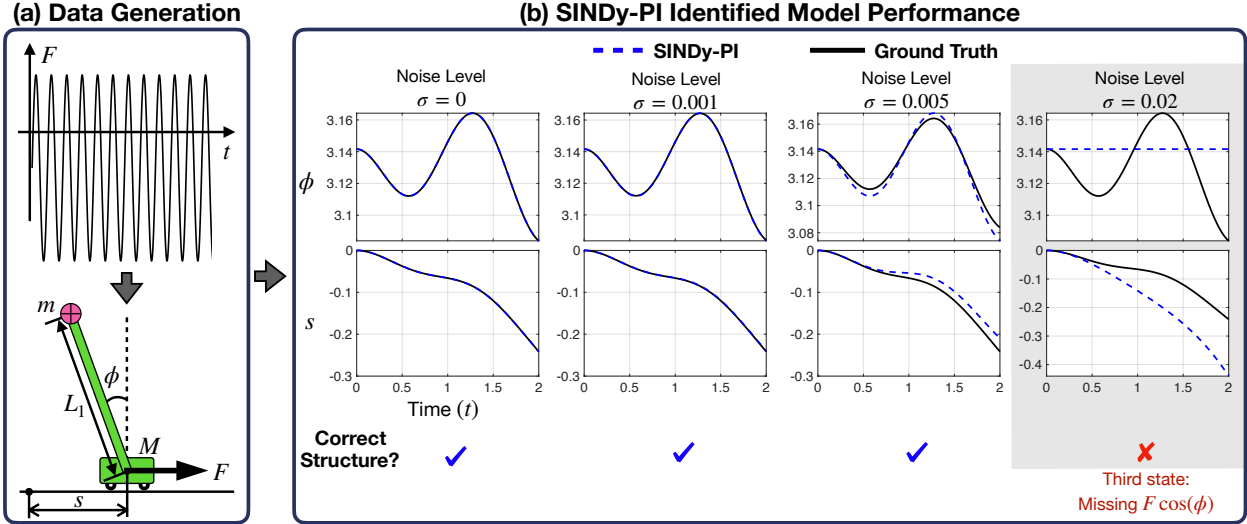


Figure 7: SINDy-PI is used to identify the single pendulum on a cart system. Control is applied to the cart, and both the cart and pendulum states are measured. When the measurement noise is small, SINDy-PI can identify the correct structure of the model.

The equations of motion are given by

$$\frac{d}{dt} \phi = \dot{\phi}, \quad (21a)$$

$$\frac{d}{dt} s = \dot{s}, \quad (21b)$$

$$\frac{d}{dt} \dot{\phi} = -\frac{(M+m)g \sin(\phi) + FL_1 \cos(\phi) + mL_1^2 \sin(\phi) \cos(\phi) \dot{\phi}^2}{L_1^2(M+m-m \cos(\phi)^2)}, \quad (21c)$$

$$\frac{d}{dt} \dot{s} = \frac{mL_1^2 \sin(\phi) \dot{\phi}^2 + FL_1 + mg \sin(\phi) \cos(\phi)}{L_1(M+m-m \cos(\phi)^2)}, \quad (21d)$$

Eq. (21) is simulated with a time step of $dt = 0.001$ to generate the training and testing data for model selection. The training data is generated using an initial condition $x_{\text{train}} = [0.3, 0, 1, 0]^T$ with the control input chosen as $F_{\text{train}} = -0.2 + 0.5 \sin(6t)$, for time $t = 0$ to $t = 16$. Similarly, the validation data is generated using an initial condition $x_{\text{val}} = [0.1, 0, 0.1, 0]^T$ with the control input chosen as $F_{\text{val}} = -1 + \sin(t) + 3 \sin(2t)$, for time $t = 0$ to $t = 2$.

The library is constructed using a combination of trigonometric and polynomial terms. Around 50 different basis functions are used for the library, and around 10 terms are tested as candidate functions. We add Gaussian noise to all system states. We then test the SINDy-PI model on a testing initial condition $x_{\text{test}} = [\pi, 0, 0, 0]^T$ with control input $F_{\text{test}} = -0.5 + 0.2 \sin(t) + 0.3 \sin(2t)$ for time $t = 0$ to $t = 2$. Fig. 7 shows the resulting SINDy-PI models. The structure of the model is correctly identified up to a noise magnitude of 0.01. Beyond this noise level, the SINDy-PI identified model only has short term prediction ability.

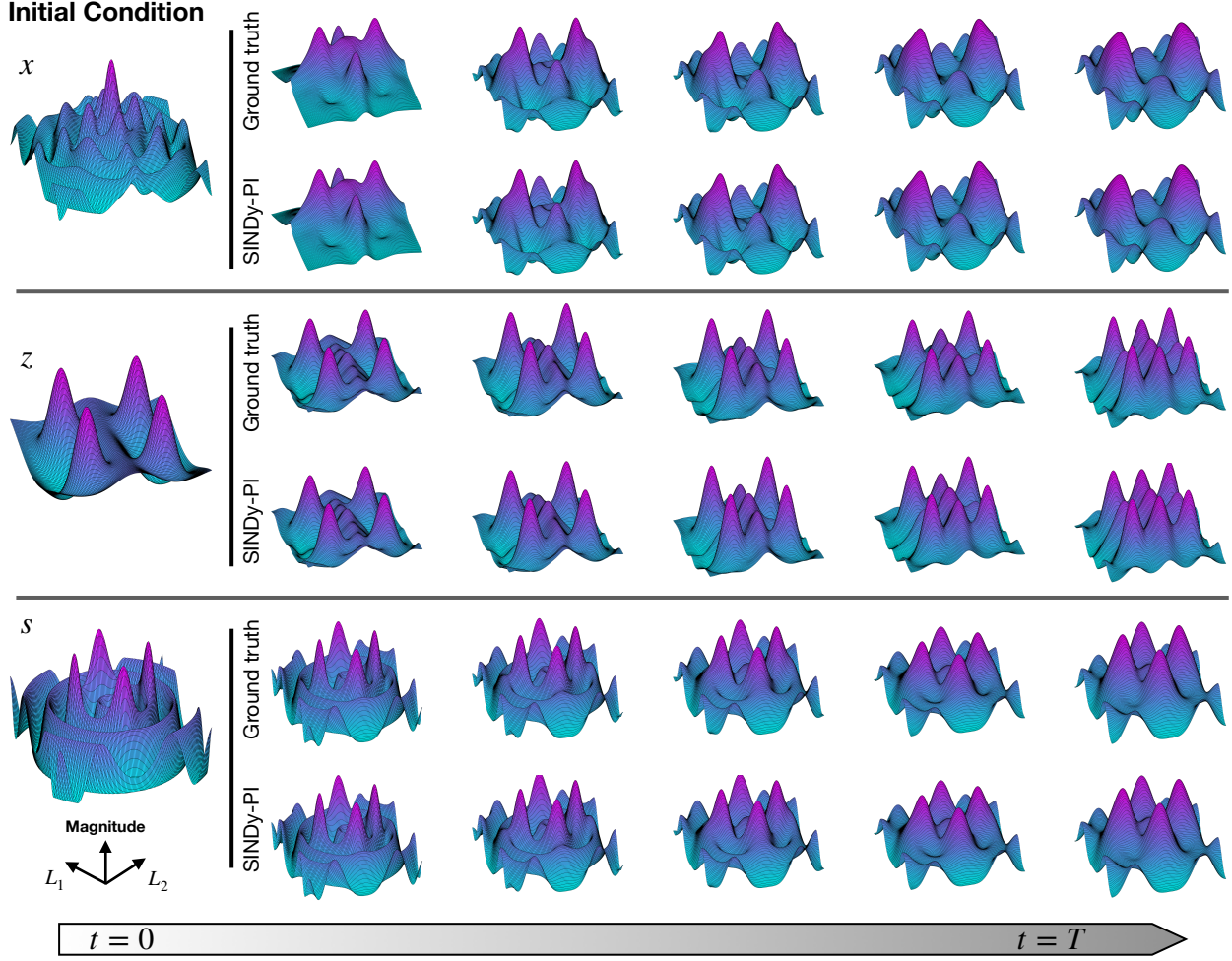


Figure 8: SINDy-PI is able to identify the simplified Belousov–Zhabotinsky reaction model.

4.3 Simplified Model of the Belousov–Zhabotinsky Reaction

We now apply SINDy-PI to a challenging PDE with rational nonlinearities, a simplified model of the Belousov–Zhabotinsky (BZ) reaction. The simplified BZ reaction model is given by [73]

$$\frac{\partial x}{\partial \tau} = \frac{1}{\varepsilon} \left(\frac{fz(q-x)}{q+x} + x - x^2 - \beta x + s \right) + \frac{D_x}{D_u} \Delta x, \quad (22a)$$

$$\frac{\partial z}{\partial \tau} = x - z - \alpha z + \gamma u + \frac{D_z}{D_u} \Delta z, \quad (22b)$$

$$\frac{\partial s}{\partial \tau} = \frac{1}{\varepsilon_2} (\beta x - s + \chi u) + \frac{D_s}{D_u} \Delta s, \quad (22c)$$

$$\frac{\partial u}{\partial \tau} = \frac{1}{\varepsilon_3} [\alpha z - (\gamma + \frac{\chi}{2}) u] + \frac{D_u}{D_u} \Delta u, \quad (22d)$$

where x , z , s , and u are dimensionless variables and $\Delta = \frac{\partial^2}{\partial x_s^2} + \frac{\partial^2}{\partial y_s^2}$ denotes the Laplacian operator.

The strong coupling dynamics and implicit behavior in (22a) make the data-driven discovery of the simplified BZ reaction challenging when using implicit-SINDy and PDE-FIND. However, SINDy-PI correctly identifies the simplified dynamics of the BZ-Reaction, as shown in Fig. 8. To generate the simplified BZ reaction data, we use a spectral method [74, 75] with time horizon $T = 1$

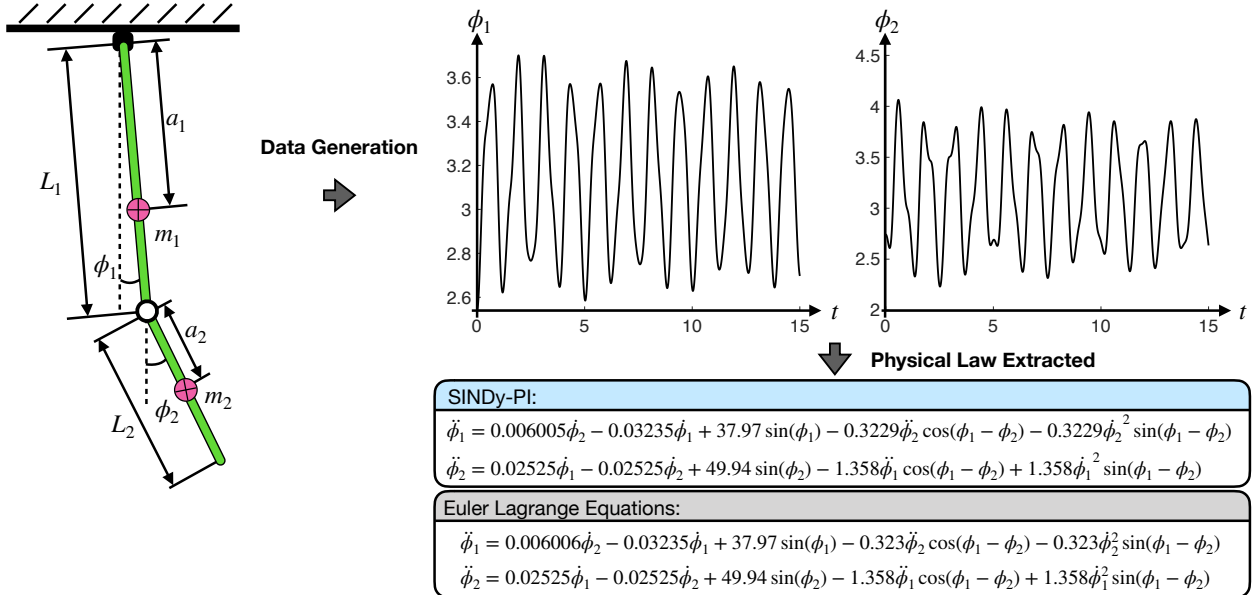


Figure 9: SINDy-PI is used to extract the conserved quantity for a double pendulum.

and time step of $dt = 0.001$. We use $n = 128$ discretization points with spatial domain ranging from -10 to 10 . The initial condition is chosen to be a mixture of Gaussian functions. 80% of the data is used for training, and the remaining 20% is used for model selection. The right-hand side library is normalized during the sparse regression process. A range of sparsity parameters λ are tested from 0.1 to 1, with increments of 0.1. The other system parameters in (22) are given in App. D and the SINDy-PI model is given in App. G.

4.4 Extracting Physical Laws and Conserved Quantities

In this final example, we demonstrate how to use SINDy-PI to extract governing physical laws and conserved quantities from data. Many systems of interest are governed by Hamiltonian or Lagrangian dynamics. Instead of identifying the ODE or PDE equations of motion, it might be possible to extract the physical laws directly. These equations contain important information about the system and may be more concise, useful, and straightforward than the underlying ODE or PDE. For example, given a Lagrangian, we can derive the equations of motion.

The most difficult aspect of using SINDy-PI to identify a physical law is how to build the library. Conservation laws may contain higher-order derivatives, such as \ddot{x} . To include all possible terms, the library size will also increase if the system has many states. Large libraries make the sparse regression sensitive to noise. Thus, extracting the physical law from data using SINDy-PI is still challenging due to the lack of constraints when constructing the library function. We only show one example in our paper to demonstrate that it is possible to achieve this using SINDy-PI, but further work is required to reduce the library size so that the sparse regression is robust.

As an example, we consider the double pendulum shown in Fig. 9, with the system parameters given in App. D. In this case, we also account for the friction in the pendulum joint, with friction constants of $k_1 = 7.2484 \times 10^{-4}$ and $k_2 = 1.6522 \times 10^{-4}$ for the pendulum arms, respectively. In this case, we extract the Lagrangian of the double pendulum [72] using SINDy-PI. To extract this Lagrangian, we simulate the system with initial condition $x_{\text{train}} = [\pi - 0.6, \pi - 0.4, 0, 0]^T$ from $t = 0$ to $t = 15$ with time step $dt = 0.001$. The resulting model is shown in Fig. 9.

5 Conclusions and Future Work

In this paper, we develop SINDy-PI (parallel,implicit), a robust variant of the SINDy algorithm to identify implicit dynamics and rational nonlinearities. SINDy-PI overcomes the sensitivity of the previous implicit-SINDy approach, which is based on a null-space calculation, making it highly sensitive to noise. Instead, we introduce both parallel and constrained optimizations to test candidate terms in the dynamics, making the new SINDy-PI algorithm as robust as the original SINDy algorithm. We also extend the algorithm to incorporate external forcing and actuation, making it more applicable to real-world systems. We demonstrate this approach on several challenging systems with implicit and rational dynamics, including ODEs, actuated systems, and PDEs. In particular, we discover the implicit dynamics for a simplified model for the BZ chemical reaction PDE, the double pendulum mechanical system, and the yeast glycolysis model, which have all been challenging test cases for advanced identification techniques. Throughout these examples, we demonstrate considerable noise robustness and reductions to the data required, over the previous implicit-SINDy algorithm.

Despite the advances outlined here, there are still many important avenues of future work. One limitation of this approach, and of SINDy in general, is in the design of the library of candidate functions. The goal is a descriptive library, but the library size grows rapidly, which in turn makes the sparse regression ill-conditioned; other issues effecting robustness are discussed in App. I. Recently, tensor approaches have been introduced to alleviate this issue, making libraries both descriptive and tractable [45], and this is a promising approach that may be incorporated in SINDy-PI as well. More generally, automatic library generation, guided by expert knowledge, is an important topic. Other research directions will involve parameterizing elements of the library, so that the algorithm simultaneously identifies the model structure and the parameters of the sparsely selected terms. Recent unified optimization frameworks, such as SR3 [59, 60], may make this possible. Model selection is another key area that will require focused attention. Balancing accuracy on test data, sparsity of the model, and the potential for overfitting are all serious concerns. The sparse regression and optimization may also be improved for better noise robustness. Finally, modifying SINDy-PI to incorporate prior physical knowledge and to only model the discrepancy with an existing model [76] will be the focus of ongoing work.

Acknowledgments

SLB acknowledges support from the Army Research Office (ARO W911NF-19-1-0045) and the Air Force Office of Scientific Research (AFOSR FA9550-18-1-0200). JNK acknowledges support from the Air Force Office of Scientific Research (AFOSR FA9550-17-1-0329). We also acknowledge valuable discussions with Aditya Nair, Eurika Kaiser, Brian DeSilva, Tony Piaskowy, Jared Callaham, and Benjamin Herrmann. We thank Ariana Mendible for reviewing the manuscript and providing useful suggestions.

References

- [1] S. L. Brunton and J. N. Kutz, *Data-Driven Science and Engineering: Machine Learning, Dynamical Systems, and Control*. Cambridge University Press, 2019.
- [2] O. Nelles, *Nonlinear system identification: from classical approaches to neural networks and fuzzy models*. Springer, 2013.
- [3] L. Ljung, “Perspectives on system identification,” *Annual Reviews in Control*, vol. 34, no. 1, pp. 1–12, 2010.

- [4] P. J. Schmid, "Dynamic mode decomposition of numerical and experimental data," *Journal of Fluid Mechanics*, vol. 656, pp. 5–28, Aug. 2010.
- [5] J. N. Kutz, S. L. Brunton, B. W. Brunton, and J. L. Proctor, *Dynamic Mode Decomposition: Data-Driven Modeling of Complex Systems*. SIAM, 2016.
- [6] M. Budinić, R. Mohr, and I. Mezić, "Applied Koopmanism a)," *Chaos: An Interdisciplinary Journal of Nonlinear Science*, vol. 22, no. 4, p. 047510, 2012.
- [7] I. Mezić, "Analysis of fluid flows via spectral properties of the Koopman operator," *Annual Review of Fluid Mechanics*, vol. 45, pp. 357–378, 2013.
- [8] M. O. Williams, I. G. Kevrekidis, and C. W. Rowley, "A data-driven approximation of the Koopman operator: extending dynamic mode decomposition," *Journal of Nonlinear Science*, vol. 6, pp. 1307–1346, 2015.
- [9] S. Klus, F. Nüske, P. Koltai, H. Wu, I. Kevrekidis, C. Schütte, and F. Noé, "Data-driven model reduction and transfer operator approximation," *Journal of Nonlinear Science*, 2018.
- [10] H. Akaike, "Fitting autoregressive models for prediction," *Ann Inst Stat Math*, vol. 21, no. 1, pp. 243–247, 1969.
- [11] S. A. Billings, *Nonlinear system identification: NARMAX methods in the time, frequency, and spatio-temporal domains*. John Wiley & Sons, 2013.
- [12] L. Yang, D. Zhang, and G. E. Karniadakis, "Physics-informed generative adversarial networks for stochastic differential equations," *arXiv preprint arXiv:1811.02033*, 2018.
- [13] C. Wehmeyer and F. Noé, "Time-lagged autoencoders: Deep learning of slow collective variables for molecular kinetics," *The Journal of Chemical Physics*, vol. 148, no. 241703, pp. 1–9, 2018.
- [14] A. Mardt, L. Pasquali, H. Wu, and F. Noé, "VAMPnets: Deep learning of molecular kinetics," *Nature Communications*, vol. 9, no. 5, 2018.
- [15] P. R. Vlachas, W. Byeon, Z. Y. Wan, T. P. Sapsis, and P. Koumoutsakos, "Data-driven forecasting of high-dimensional chaotic systems with long short-term memory networks," *Proc. R. Soc. A*, vol. 474, no. 2213, p. 20170844, 2018.
- [16] J. Pathak, B. Hunt, M. Girvan, Z. Lu, and E. Ott, "Model-free prediction of large spatiotemporally chaotic systems from data: a reservoir computing approach," *Physical review letters*, vol. 120, no. 2, p. 024102, 2018.
- [17] L. Lu, X. Meng, Z. Mao, and G. E. Karniadakis, "Deepxde: A deep learning library for solving differential equations," *arXiv preprint arXiv:1907.04502*, 2019.
- [18] M. Raissi, P. Perdikaris, and G. Karniadakis, "Physics-informed neural networks: A deep learning framework for solving forward and inverse problems involving nonlinear partial differential equations," *Journal of Computational Physics*, vol. 378, pp. 686–707, 2019.
- [19] K. Champion, B. Lusch, J. N. Kutz, and S. L. Brunton, "Data-driven discovery of coordinates and governing equations," *Proceedings of the National Academy of Sciences*, vol. 116, no. 45, pp. 22 445–22 451, 2019.
- [20] M. Raissi, A. Yazdani, and G. E. Karniadakis, "Hidden fluid mechanics: Learning velocity and pressure fields from flow visualizations," *Science*, vol. 367, no. 6481, pp. 1026–1030, 2020.
- [21] M. Raissi and G. E. Karniadakis, "Machine learning of linear differential equations using gaussian processes," *arXiv preprint arXiv:1701.02440*, 2017.
- [22] ——, "Hidden physics models: Machine learning of nonlinear partial differential equations," *Journal of Computational Physics*, vol. 357, pp. 125–141, 2018.
- [23] D. Giannakis and A. J. Majda, "Nonlinear laplacian spectral analysis for time series with intermittency and low-frequency variability," *Proceedings of the National Academy of Sciences*, vol. 109, no. 7, pp. 2222–2227, 2012.
- [24] O. Yair, R. Talmon, R. R. Coifman, and I. G. Kevrekidis, "Reconstruction of normal forms by learning informed observation geometries from data," *Proceedings of the National Academy of Sciences*, p. 201620045, 2017.
- [25] J. Bongard and H. Lipson, "Automated reverse engineering of nonlinear dynamical systems," *Proc. Natl. Acad. Sciences*, vol. 104, no. 24, pp. 9943–9948, 2007.
- [26] M. Schmidt and H. Lipson, "Distilling free-form natural laws from experimental data," *Science*, vol. 324, no. 5923, pp. 81–85, 2009.
- [27] B. C. Daniels and I. Nemenman, "Automated adaptive inference of phenomenological dynamical models," *Nature communications*, vol. 6, 2015.
- [28] S. L. Brunton, J. L. Proctor, and J. N. Kutz, "Discovering governing equations from data by sparse identification of nonlinear dynamical systems," *Proceedings of the national academy of sciences*, vol. 113,

- no. 15, pp. 3932–3937, 2016.
- [29] S. H. Rudy, S. L. Brunton, J. L. Proctor, and J. N. Kutz, “Data-driven discovery of partial differential equations,” *Science Advances*, vol. 3, no. 4, p. e1602614, 2017.
 - [30] H. Schaeffer, “Learning partial differential equations via data discovery and sparse optimization,” in *Proc. R. Soc. A*, vol. 473, no. 2197. The Royal Society, 2017, p. 20160446.
 - [31] M. Sorokina, S. Sygletos, and S. Turitsyn, “Sparse identification for nonlinear optical communication systems: SINO method,” *Optics express*, vol. 24, no. 26, pp. 30 433–30 443, 2016.
 - [32] M. Dam, M. Brøns, J. Juul Rasmussen, V. Naulin, and J. S. Hesthaven, “Sparse identification of a predator-prey system from simulation data of a convection model,” *Physics of Plasmas*, vol. 24, no. 2, p. 022310, 2017.
 - [33] A. Narasingam and J. S.-I. Kwon, “Data-driven identification of interpretable reduced-order models using sparse regression,” *Computers & Chemical Engineering*, vol. 119, pp. 101–111, 2018.
 - [34] J.-C. Loiseau and S. L. Brunton, “Constrained sparse galerkin regression,” *Journal of Fluid Mechanics*, vol. 838, pp. 42–67, 2018.
 - [35] M. Quade, M. Abel, J. N. Kutz, and S. L. Brunton, “Sparse identification of nonlinear dynamics for rapid model recovery,” *To appear in chaos*, 2018.
 - [36] L. Boninsegna, F. Nüske, and C. Clementi, “Sparse learning of stochastic dynamical equations,” *The Journal of Chemical Physics*, vol. 148, no. 24, p. 241723, 2018.
 - [37] J.-C. Loiseau, B. R. Noack, and S. L. Brunton, “Sparse reduced-order modelling: sensor-based dynamics to full-state estimation,” *Journal of Fluid Mechanics*, vol. 844, pp. 459–490, 2018.
 - [38] L. Zhang and H. Schaeffer, “On the convergence of the SINDy algorithm,” *arXiv preprint arXiv:1805.06445*, 2018.
 - [39] M. Hoffmann, C. Fröhner, and F. Noé, “Reactive SINDy: Discovering governing reactions from concentration data,” *Journal of Chemical Physics*, vol. 150, no. 025101, 2019.
 - [40] N. M. Mangan, T. Askham, S. L. Brunton, J. N. Kutz, and J. L. Proctor, “Model selection for hybrid dynamical systems via sparse regression,” *Proceedings of the Royal Society A*, vol. 475, no. 2223, p. 20180534, 2019.
 - [41] S. Thaler, L. Paehler, and N. A. Adams, “Sparse identification of truncation errors,” *Journal of Computational Physics*, vol. 397, p. 108851, 2019.
 - [42] Z. Lai and S. Nagarajaiah, “Sparse structural system identification method for nonlinear dynamic systems with hysteresis/inelastic behavior,” *Mechanical Systems and Signal Processing*, vol. 117, pp. 813–842, 2019.
 - [43] K. Wu and D. Xiu, “Numerical aspects for approximating governing equations using data,” *Journal of Computational Physics*, vol. 384, pp. 200–221, 2019.
 - [44] B. de Silva, D. M. Higdon, S. L. Brunton, and J. N. Kutz, “Discovery of physics from data: Universal laws and discrepancies,” *arXiv preprint arXiv:1906.07906*, 2019.
 - [45] P. Gelß, S. Klus, J. Eisert, and C. Schütte, “Multidimensional approximation of nonlinear dynamical systems,” *Journal of Computational and Nonlinear Dynamics*, vol. 14, no. 6, 2019.
 - [46] S. Zhang and G. Lin, “Robust data-driven discovery of governing physical laws with error bars,” *Proceedings of the Royal Society A: Mathematical, Physical and Engineering Sciences*, vol. 474, no. 2217, p. 20180305, 2018.
 - [47] N. M. Mangan, S. L. Brunton, J. L. Proctor, and J. N. Kutz, “Inferring biological networks by sparse identification of nonlinear dynamics,” *IEEE Transactions on Molecular, Biological and Multi-Scale Communications*, vol. 2, no. 1, pp. 52–63, 2016.
 - [48] E. Kaiser, J. N. Kutz, and S. L. Brunton, “Sparse identification of nonlinear dynamics for model predictive control in the low-data limit,” *Proceedings of the Royal Society of London A*, vol. 474, no. 2219, 2018.
 - [49] H. Schaeffer and S. G. McCalla, “Sparse model selection via integral terms,” *Physical Review E*, vol. 96, no. 2, p. 023302, 2017.
 - [50] P. A. Reinbold, D. R. Gurevich, and R. O. Grigoriev, “Using noisy or incomplete data to discover models of spatiotemporal dynamics,” *Physical Review E*, vol. 101, no. 1, p. 010203, 2020.
 - [51] J. Wright, A. Yang, A. Ganesh, S. Sastry, and Y. Ma, “Robust face recognition via sparse representation,” *IEEE Transactions on Pattern Analysis and Machine Intelligence (PAMI)*, vol. 31, no. 2, pp. 210–227, 2009.
 - [52] Q. Qu, J. Sun, and J. Wright, “Finding a sparse vector in a subspace: Linear sparsity using alternating directions,” in *Proceedings of the 27th International Conference on Neural Information Processing Systems - Volume 2*, ser. NIPS’14. Cambridge, MA, USA: MIT Press, 2014, p. 3401–3409.
 - [53] Q. Zhu, Y. Wang, D. Zhao, S. Li, and S. A. Billings, “Review of rational (total) nonlinear dynamic

- system modelling, identification, and control," *International Journal of Systems Science*, vol. 46, no. 12, pp. 2122–2133, 2015.
- [54] Q. Zhu, L. Liu, W. Zhang, and S. Li, "Control of complex nonlinear dynamic rational systems," *Complexity*, vol. 2018, 2018.
- [55] I. Koryakovskiy, M. Kudruss, H. Vallery, R. Babuška, and W. Caarls, "Model-plant mismatch compensation using reinforcement learning," *IEEE Robotics and Automation Letters*, vol. 3, no. 3, pp. 2471–2477, 2018.
- [56] R. Chartrand, "Numerical differentiation of noisy, nonsmooth data," *ISRN Applied Mathematics*, vol. 2011, 2011.
- [57] L. Zhang and H. Schaeffer, "On the convergence of the sindy algorithm," *Multiscale Modeling & Simulation*, vol. 17, no. 3, pp. 948–972, 2019.
- [58] R. Tibshirani, "Regression shrinkage and selection via the lasso," *Journal of the Royal Statistical Society: Series B (Methodological)*, vol. 58, no. 1, pp. 267–288, 1996.
- [59] P. Zheng, T. Askham, S. L. Brunton, J. N. Kutz, and A. Y. Aravkin, "A unified framework for sparse relaxed regularized regression: SR3," *IEEE Access*, vol. 7, pp. 1404–1423, 2018.
- [60] K. Champion, A. Zheng, Peng Aravkin, S. Brunton, and J. Nathan Kutz, "A unified sparse optimization framework to learn parsimonious physics-informed models from data," *arxiv*, vol. 0, p. 1906.10612v1, 2019.
- [61] W. Pan, Y. Yuan, J. Gonçalves, and G. Stan, "A sparse Bayesian approach to the identification of nonlinear state-space systems," *IEEE Transactions on Automatic Control*, vol. 61, no. 1, pp. 182–187, January 2016.
- [62] M. Gavish and D. L. Donoho, "The optimal hard threshold for singular values is $4/\sqrt{3}$," *IEEE Transactions on Information Theory*, vol. 60, no. 8, pp. 5040–5053, 2014.
- [63] H. Akaike, "Information theory and an extension of the maximum likelihood principle," in *Selected papers of hirotugu akaike*. Springer, 1998, pp. 199–213.
- [64] ———, "A new look at the statistical model identification," *IEEE transactions on automatic control*, vol. 19, no. 6, pp. 716–723, 1974.
- [65] G. Schwarz, "Estimating the dimension of a model," *Ann. Statist.*, vol. 6, no. 2, pp. 461–464, 03 1978. [Online]. Available: <https://doi.org/10.1214/aos/1176344136>
- [66] N. M. Mangan, J. N. Kutz, S. L. Brunton, and J. L. Proctor, "Model selection for dynamical systems via sparse regression and information criteria," *Proceedings of the Royal Society A: Mathematical, Physical and Engineering Sciences*, vol. 473, no. 2204, p. 20170009, 2017.
- [67] M. Grant and S. Boyd, "CVX: Matlab software for disciplined convex programming, version 2.1," <http://cvxr.com/cvx>, Mar. 2014.
- [68] ———, "Graph implementations for nonsmooth convex programs," in *Recent Advances in Learning and Control*, ser. Lecture Notes in Control and Information Sciences, V. Blondel, S. Boyd, and H. Kimura, Eds. Springer-Verlag Limited, 2008, pp. 95–110, http://stanford.edu/~boyd/graph_dcp.html.
- [69] K. A. Johnson and R. S. Goody, "The original Michaelis constant: Translation of the 1913 Michaelis-Menten paper," *Biochemistry*, vol. 50, no. 39, pp. 8264–8269, 2011.
- [70] A. Cornish-Bowden, "One hundred years of Michaelis–Menten kinetics," *Perspectives in Science*, vol. 4, pp. 3–9, 2015.
- [71] M. D. Schmidt, R. R. Vallabhajosyula, J. W. Jenkins, J. E. Hood, A. S. Soni, J. P. Wikswo, and H. Lipson, "Automated refinement and inference of analytical models for metabolic networks," *Physical biology*, vol. 8, no. 5, p. 055011, 2011.
- [72] K. Graichen, M. Treuer, and M. Zeitz, "Swing-up of the double pendulum on a cart by feedforward and feedback control with experimental validation," *Automatica*, vol. 43, no. 1, pp. 63 – 71, 2007.
- [73] V. K. Vanag, "Waves and patterns in reaction–diffusion systems. Belousov–Zhabotinsky reaction in water-in-oil microemulsions," *Physics-Uspekhi*, vol. 47, no. 9, p. 923, 2004.
- [74] *Spectral Methods in MATLAB*. SIAM, 2000, vol. 10, ch. 8. Chebyshev Series and the FFT, pp. 75–86. [Online]. Available: <https://pubs.siam.org/doi/abs/10.1137/1.9780898719598.ch8>
- [75] J. N. Kutz, *Data-driven modeling & scientific computation: methods for complex systems & big data*. Oxford University Press, 2013.
- [76] K. Kaheman, E. Kaiser, B. Strom, J. N. Kutz, and S. L. Brunton, "Learning discrepancy models from experimental data," *arXiv preprint arXiv:1909.08574*, 2019.
- [77] M. C. Kennedy and A. O'Hagan, "Bayesian calibration of computer models," *Journal of the Royal Statistical Society: Series B (Statistical Methodology)*, vol. 63, no. 3, pp. 425–464, 2001.
- [78] P. D. Arendt, D. W. Apley, and W. Chen, "Quantification of model uncertainty: Calibration, model

discrepancy, and identifiability," *Journal of Mechanical Design*, vol. 134, no. 10, 2012.

A Noise Sensitivity of SINDy-PI and implicit-SINDy

A.1 Performance Evaluation Criteria

To compare the performance of SINDy-PI and implicit-SINDy for noisy data, we must define an evaluation criteria. We compare the performance of the best model generated by each method that has the lowest prediction error on the test data, selected according to Eq. (13). To compare the models generated by the two methods with the ground truth model, we use the concept of model discrepancy [76–78] and set prediction accuracy, structural accuracy, and parameter accuracy as our performance criteria. A good prediction error does not guarantee the model has good structural accuracy and parameter accuracy, and vice versa, motivating multiple performance criteria.

A.2 Numerical Experiments

We use the Michaelis–Menten kinetics, given by Eq. (18), to compare the performance of SINDy-PI and implicit-SINDy. We performed our numerical experiments as follows:

- Step 1: Randomly generate 2400 different initial conditions of different magnitudes ranging from 0 to 12.5. Simulate those initial conditions using a fourth-order Runge–Kutta method with time step $dt = 0.1$ and time horizon $T = 5$. The testing data is generated using 600 random initial conditions using the same method as the training data.
- Step 2: Add Gaussian noise to the training and testing data. 23 different Gaussian noise levels with magnitudes ranging from 10^{-7} to 5×10^{-1} are used. For each noise level, 30 different random noise realizations are generated, resulting in 30 different noisy data sets for each noise level.
- Step 3: Compute the derivative of the noisy data. We investigate several approaches, including finite-difference and total-variation regularized difference (TVRegDiff) [56] derivatives. In all cases, SINDy-PI is several orders of magnitude more robust to noise than implicit-SINDy, and only the result of using TVRegDiff is shown in this paper. TVRegDiff generates more accurate derivatives, but also requires hyperparameter tuning and causes aliasing, so we trim the ends of the time series generated by each initial condition (first and last 30%). It is possible to add Gaussian noise to the clean derivative data to investigate robustness, although this is less relevant for real-world scenarios, where only noisy state data is available.

- Step 4: Train SINDy-PI and implicit-SINDy models on noisy training data. For each noise level, we sweep through 68 different sparsity parameters λ for SINDy-PI, from 0.01 to 5. The λ is varied by a factor of 2 [52] to calculate the null space in the implicit-SINDy method. The library for implicit-SINDy and SINDy-PI is

$$\Theta(\mathbf{X}, \dot{\mathbf{X}}) = [\mathbf{1} \ \mathbf{X} \ \mathbf{X}^2 \ \mathbf{X}^3 \ \mathbf{X}^4 \ \dot{\mathbf{X}} \ \dot{\mathbf{X}}\mathbf{X} \ \dot{\mathbf{X}}\mathbf{X}^2 \ \dot{\mathbf{X}}\mathbf{X}^3 \ \dot{\mathbf{X}}\mathbf{X}^4]. \quad (23)$$

- Step 5: Due to the various parameter values, we use model selection to choose a model. We use the test data with the same noise magnitude to perform the model selection process. The ratio of training data and testing data is 8 : 2.

Table 1: The parameter used for simulating the Eq. (19).

Parameter	c_1	c_2	c_3	d_1	d_2	d_3	d_4	e_1	e_2	e_3	e_4	f_1	f_2
Value	2.5	-100	13.6769	200	13.6769	-6	-6	6	-64	6	16	64	-13
Parameter	f_3	f_4	f_5	g_1	g_2	h_1	h_2	h_3	h_4	h_5	j_1	j_2	j_3
Value	13	-16	-100	1.3	-3.1	-200	13.6769	128	-1.28	-32	6	-18	-100

Step 6: The best model generated by the two methods are compared. We use the prediction error, error in the model structure (i.e., the number of terms that are incorrectly present or missing from the model), and parameter error as our model performance evaluation criteria. We average the performance over 30 different noise realizations for each noise level. We then plot the distribution of structure error in Fig. 3.

Many parameters affect the performance of these methods: the length of training data, prediction steps to calculate prediction error, the initial conditions for training data, choice of the library, and the derivative computation. We have attempted to carefully optimize each method, although an exhaustive parameter sweep is beyond the scope of the present work. However, in all cases SINDy-PI outperforms implicit-SINDy.

B Data Usage of SINDy-PI and implicit-SINDy

Sec. 3.4 investigates the data usage of SINDy-PI and implicit-SINDy on the yeast glycolysis model in Eq. (19). The parameters of this problems are given in Table. 1. The data usage comparison is performed by the following steps:

Step 1: Generate training data by simulating Eq. (19) with parameters in Table. 1 and a time step of $dt = 0.1$, with time horizon $T = 5$. We simulate the system using 900 random initial conditions with magnitude ranging from 0 to 3.

Step 2: Shuffle the training data and select j percent of the entire training data set at random to train the SINDy-PI and implicit-SINDy models. These training data are sampled from all trajectories, and they are not necessarily consecutive in time. No noise is added since we only care about the effect of the data length in this case. The sparsity parameter λ is fixed for both algorithms (different values); this value is selected for a single percentage j where both methods fail to identify the correct model, and we sweep through λ .

Step 3: Run the numerical experiment for 20 times for each data length and calculate the percentage of times the two algorithms yield the correct structure of the Eq. (19f).

The final comparison is shown in Fig. 4. Data usage requirements for other state equations are given in Table 2; Fig. 4 shows results for the hardest equation to identify. The other equations require less data. Normalizing the SINDy-PI library improves data learning rates as well.

C SINDy-PI and PDE-FIND on Rational PDE Problem

In Sec. 3.5, we compared the performance of SINDy-PI and PDE-FIND on a modified KdV equation. The simulation data is obtained using a spectral method [74] with a time step of $dt = 0.01$ and time horizon $T = 20$, spatial domain $L = -25$ to 25, and $n = 128$ spatial discretization points.

Table 2: Comparison of data usage of SINDy-PI and implicit-SINDy on other states.

	Equation	Eq. (19a)	Eq. (19b)	Eq. (19c)	Eq. (19d)	Eq. (19e)	Eq. (19f)	Eq. (19g)
	Library Order	6	6	3	3	3	6	3
SINDy-PI un-normalized	Left-Hand Side	\dot{x}_1	$\dot{x}_1 x_6^4$	\dot{x}_2	$\dot{x}_2 x_6^4$	\dot{x}_3	\dot{x}_4	\dot{x}_5
	Threshold	0.5	0.05	0.5	0.05	0.2	0.5	0.3
	Data Usage	50%	7.5%	55%	8.5%	0.5%	0.5%	40%
SINDy-PI normalized	Left-Hand Side	\dot{x}_1	$\dot{x}_1 x_6^4$	\dot{x}_2	$\dot{x}_2 x_6^4$	\dot{x}_3	\dot{x}_4	\dot{x}_5
	Threshold	0.5	0.5	0.5	0.5	0.6	0.8	0.4
	Data Usage	18%	3%	10%	3%	0.45%	0.45%	0.275%
implicit-SINDy normalized	Threshold	5×10^{-3}		2×10^{-3}		8×10^{-3}	8×10^{-3}	8×10^{-3}
	Data Usage	10%		10%		0.5%	0.6%	0.3%

The library of PDE-FIND is chosen to be

$$\Theta(\mathbf{U}, \mathbf{U}_x, \mathbf{U}_{xx}, \mathbf{U}_{xxx}) = [\mathbf{1} \ \mathbf{U} \ \mathbf{U}_x \ \mathbf{U}_{xx} \ \mathbf{U}_{xxx} \ \mathbf{U}_x^2 \ \mathbf{U}_{xx}^2 \ \mathbf{U}_{xxx}^2 \ \mathbf{U} \ \mathbf{U}_x \\ \mathbf{U} \ \mathbf{U}_{xx} \ \mathbf{U} \ \mathbf{U}_{xxx} \ \mathbf{U}^2 \ \mathbf{U}_x^2 \ \mathbf{U}^2 \ \mathbf{U}_{xx}^2 \ \mathbf{U}^2 \ \mathbf{U}_{xxx}^2], \quad (24)$$

and the right-hand side library for the SINDy-PI is chosen to be

$$\Theta(\mathbf{U}, \mathbf{U}_x, \mathbf{U}_{xx}, \mathbf{U}_{xxx}) = [\mathbf{1} \ \mathbf{U} \ \mathbf{U}_t \ \mathbf{U}_x \ \mathbf{U}_{xx} \ \mathbf{U}_{xxx} \ \mathbf{U}^2 \ \mathbf{U}_t^2 \ \mathbf{U}_x^2 \ \mathbf{U}_{xx}^2 \ \mathbf{U}_{xxx}^2 \\ \mathbf{U} \ \mathbf{U}_t \ \mathbf{U} \ \mathbf{U}_x \ \mathbf{U} \ \mathbf{U}_{xx} \ \mathbf{U} \ \mathbf{U}_{xxx} \ \mathbf{U}^2 \ \mathbf{U}_x^2 \ \mathbf{U}^2 \ \mathbf{U}_{xx}^2 \ \mathbf{U}^2 \ \mathbf{U}_{xxx}^2], \quad (25)$$

while the left-hand side library is chosen to be

$$C(\mathbf{U}, \mathbf{U}_t, \mathbf{U}_x, \mathbf{U}_{xx}) = [\mathbf{U}_t \ \mathbf{U} \ \mathbf{U}_t \ \mathbf{U} \ \mathbf{U}_x \ \mathbf{U} \ \mathbf{U}_{xx}]. \quad (26)$$

For both SINDy-PI and PDE-FIND, we used 100 different values for the sparsity parameter λ ranging from 0.1 to 10 with step size 0.1. We use 80% of the simulation data for training and 20% for testing and model selection. We calculate the normalized prediction error for all models on state u_t and the model with minimum prediction error is selected as the final model.

D Parameter Values for Simulations

The parameters for the double pendulum simulation in Sec. 4.1 are given in Table 3. The parameters used to simulate the simplified model of the Belousov-Zhabotinsky reaction in Eq. (22) are given in Table 5.

Table 3: Parameters used to simulate the double pendulum.

Parameter	m_1	m_2	L_1	L_2	a_1	a_2	I_1	I_2	g
Value	0.2704	0.2056	0.2667	0.2667	0.191	0.1621	0.003	0.0011	9.81

Table 4: Parameters used to simulate the single pendulum on a cart.

Parameter	m	L	M	g
Value	1	1	1	9.81

Table 5: Parameters Used in Eq. (22) for Simulating the Belousov-Zhabotinsky Reaction Model.

Parameter	q	f	ε	α	β	γ	ε_2	ε_3	χ	D_x	D_z	D_s	D_u
Value	1	1.5	0.3	0.3	0.26	0.4	0.15	0.03	0	0.01	0.01	1	1

E SINDy-PI Models for the Single Pendulum on a Cart

The Lagrangian for the single pendulum on a cart with an input force on the cart is:

$$\mathcal{L} = T - V = \frac{1}{2}(m + M)\dot{s}^2 + \frac{1}{2}L^2m\dot{\phi}^2 - Lgm\cos(\phi) + Lm\cos(\phi)\dot{\phi}\dot{s}, \quad (27)$$

where m is the mass at the end of the pendulum arm, M is the mass of the cart, L is the length of the pendulum arm, s is the position of the cart, and ϕ is the pendulum angle. We do not consider damping in this case. Using the numeric values $m = M = L = 1$ and $g = -9.81$ this simplifies to

$$\mathcal{L} = T - V = \dot{s}^2 + \frac{1}{2}\dot{\phi}^2 - 9.81\cos(\phi) + \cos(\phi)\dot{\phi}\dot{s}, \quad (28)$$

The Euler-Lagrange equation of the system are

$$\begin{aligned} \frac{d}{dt} \frac{\partial \mathcal{L}}{\partial \dot{\phi}} - \frac{\partial \mathcal{L}}{\partial \phi} &= 0, & mL^2\ddot{\phi} + mL\ddot{s}\cos(\phi) - Lgm\sin(\phi) &= 0 \\ \frac{d}{dt} \frac{\partial \mathcal{L}}{\partial \dot{s}} - \frac{\partial \mathcal{L}}{\partial s} &= F, & (M+m)\ddot{s} - F - mL\sin(\phi)\dot{\phi}^2 + mL\ddot{\phi}\cos(\phi) &= 0 \end{aligned} \quad (29a)$$

where F is the force applied to the pendulum cart. It is possible to isolate $\ddot{\phi}$ and \ddot{s} :

$$\ddot{\phi} = \frac{-(F\cos(\phi) - Mg\sin(\phi) - mg\sin(\phi) + Lm\cos(\phi)\sin(\phi)\dot{\phi}^2)}{L(M+m\sin(\phi)^2)}, \quad (30a)$$

$$\ddot{s} = \frac{F + Lm\sin(\phi)\dot{\phi}^2 - mg\cos(\phi)\sin(\phi)}{M + m\sin(\phi)^2}. \quad (30b)$$

It is possible to write this as a system of four coupled first-order equations

$$\frac{d}{dt}\phi = \dot{\phi}, \quad (31a)$$

$$\frac{d}{dt}s = \dot{s}, \quad (31b)$$

$$\frac{d}{dt}\dot{\phi} = \frac{-(F\cos(\phi) - Mg\sin(\phi) - mg\sin(\phi) + Lm\cos(\phi)\sin(\phi)\dot{\phi}^2)}{L(M+m\sin(\phi)^2)}, \quad (31c)$$

$$\frac{d}{dt}\dot{s} = \frac{F + Lm\sin(\phi)\dot{\phi}^2 - mg\cos(\phi)\sin(\phi)}{M + m\sin(\phi)^2}. \quad (31d)$$

With the numerical values shown in Table. 4, this becomes

$$\frac{d}{dt}\phi = \dot{\phi}, \quad (32a)$$

$$\frac{d}{dt}s = \dot{s}, \quad (32b)$$

$$\frac{d}{dt}\dot{\phi} = \frac{19.62\sin(\phi) - F\cos(\phi) - \sin(\phi)\cos(\phi)\dot{\phi}^2}{2 - \cos(\phi)^2}, \quad (32c)$$

$$\frac{d}{dt}\dot{s} = \frac{2F - 9.81\sin(2\phi) + 2\sin(\phi)\dot{\phi}^2}{2 + 2\sin(\phi)^2}. \quad (32d)$$

Parameters identified by SINDy-PI under different noise magnitudes are presented in Tables 6 and 7.

Table 6: Parameters identified by SINDy-PI for Eq. (32c) under different noise magnitudes.

Value Noise Magnitude	Basis	Numerator			Denominator	
		$\sin(\phi)$	$F \cos(\phi)$	$\sin(\phi) \cos(\phi) \dot{\phi}^2$	Constant	$\cos(\phi)^2$
0	19.62	-1	-1	2	-1	
0.001	19.618	-1.0005	-0.9999	2	-1	
0.005	19.6135	-1.171	-0.9996	2	-0.9997	
0.02	19.5881	Not Identified	-0.4912	2	-1.0122	

Table 7: Parameters identified by SINDy-PI for Eq. (32d) under different noise magnitudes.

Value Noise Magnitude	Basis	Numerator			Denominator	
		F	$\sin(2\phi)$	$\sin(\phi)\dot{\phi}^2$	Constant	$\sin(\phi)^2$
0	2	-9.81	2	2	2	
0.001	1.9992	-9.816	1.9992	2	1.9992	
0.005	1.9982	-9.8015	1.9986	2	1.9986	
0.02	2.0705	-9.8234	2.0041	2	2.0041	

F SINDy-PI Models for the Mounted Double Pendulum

For a mounted double pendulum system shown in Fig. 6 we could have following parameters: the parameters of the pendulum are center of mass m_1 and m_2 , center of mass position a_1 and a_2 , arm length L_1 and L_2 , arm inertia I_1 and I_2 , arm rotational angle ϕ_1 and ϕ_2 , gravity acceleration g . Those values could be seen from Table. 3. If we consider friction between the pendulum joint, we could define $k_1 = 7.2485 \times 10^{-4}$ and $k_2 = 1.6522 \times 10^{-4}$ as our damping coefficient. It is easy to derive the Lagrangian of the mounted double pendulum which is given by

$$\begin{aligned} \mathcal{L} = T - V = & (m_2((L_1 \cos(\phi_1)\dot{\phi}_1 + a_2 \cos(\phi_2)\dot{\phi}_2)^2 + (L_1 \sin(\phi_1)\dot{\phi}_1 + a_2 \sin(\phi_2)\dot{\phi}_2)^2))/2 + \\ & (m_1(a_1^2 \cos(\phi_1)^2 \dot{\phi}_1^2 + a_1^2 \sin(\phi_1)^2 \dot{\phi}_1^2))/2 + (I_1 \dot{\phi}_1^2)/2 + (I_2 \dot{\phi}_2^2)/2 - gm_2(a_2 \cos(\phi_2) \\ & + L_1 \cos(\phi_1)) - a_1 g m_1 \cos(\phi_1) \end{aligned} \quad (33)$$

The damping term caused by friction with friction coefficients k_1 and k_2 is

$$R_a = \frac{1}{2}k_1 \dot{\phi}_1 + \frac{1}{2}k_2(\dot{\phi}_1 - \dot{\phi}_2)^2 \quad (34)$$

The Euler-Lagrange equations with a Rayleigh dissipation term are then:

$$\frac{d}{dt} \frac{\partial \mathcal{L}}{\partial \dot{\phi}_1} - \frac{\partial \mathcal{L}}{\partial \phi_1} + \frac{\partial R_a}{\partial \dot{\phi}_1} = 0, \quad (35a)$$

$$\frac{d}{dt} \frac{\partial \mathcal{L}}{\partial \dot{\phi}_2} - \frac{\partial \mathcal{L}}{\partial \phi_2} + \frac{\partial R_a}{\partial \dot{\phi}_2} = 0. \quad (35b)$$

The symbolic form of the Eq. (35a) is

$$\begin{aligned} I_1 \ddot{\phi}_1 + k_1 \dot{\phi}_1 + k_2 \dot{\phi}_1 + L_1^2 \ddot{\phi}_1 m_2 + a_1^2 \ddot{\phi}_1 m_1 + L_1 a_2 m_2 \sin(\phi_1 - \phi_2) \dot{\phi}_2^2 \\ + L_1 a_2 \ddot{\phi}_2 m_2 \cos(\phi_1 - \phi_2) - k_2 \dot{\phi}_2 - L_1 g m_2 \sin(\phi_1) - a_1 g m_1 \sin(\phi_1) = 0, \end{aligned} \quad (36)$$

and the symbolic form of Eq. (35b) is

$$\begin{aligned} I_2 \ddot{\phi}_2 + k_2 \dot{\phi}_2 + a_2^2 \ddot{\phi}_2 m_2 + L_1 a_2 \ddot{\phi}_1 m_2 \cos(\phi_1 - \phi_2) - k_2 \dot{\phi}_1 \\ - a_2 g m_2 \sin(\phi_2) - L_1 a_2 m_2 \sin(\phi_1 - \phi_2) \dot{\phi}_1^2 = 0. \end{aligned} \quad (37)$$

Using the numerical parameter values in these equations gives

$$\begin{aligned} \ddot{\phi}_1 + 0.03235 \dot{\phi}_1 + 0.323 \ddot{\phi}_2 \cos(\phi_1 - \phi_2) + 0.323 \dot{\phi}_2^2 \sin(\phi_1 - \phi_2) - 0.006006 \dot{\phi}_2 - 37.97 \sin(\phi_1) = 0. \\ \ddot{\phi}_2 + 0.02525 \dot{\phi}_2 + 1.358 \ddot{\phi}_1 \cos(\phi_1 - \phi_2) - 0.02525 \dot{\phi}_1 - 49.94 \sin(\phi_2) - 1.358 \dot{\phi}_1^2 \sin(\phi_1 - \phi_2) = 0. \end{aligned}$$

If we set $k_1 = k_2 = 0$ and combine the equations, it is possible to solve for $\ddot{\phi}_1$ and $\ddot{\phi}_2$

$$\begin{aligned} \ddot{\phi}_1 = & (L_1 a_2^2 g m_2^2 \sin(\phi_1) - 2L_1 a_2^3 \dot{\phi}_2^2 m_2^2 \sin(\phi_1 - \phi_2) + 2I_2 L_1 g m_2 \sin(\phi_1) \\ & + L_1 a_2^2 g m_2^2 \sin(\phi_1 - 2\phi_2) + 2I_2 a_1 g m_1 \sin(\phi_1) - L_1^2 a_2^2 \dot{\phi}_1^2 m_2^2 \sin(2\phi_1 - 2\phi_2) \\ & - 2I_2 L_1 a_2 \dot{\phi}_2^2 m_2 \sin(\phi_1 - \phi_2) + 2a_1 a_2^2 g m_1 m_2 \sin(\phi_1)) / (2I_1 I_2 + L_1^2 a_2^2 m_2^2) \\ & + 2I_2 L_1^2 m_2 + 2I_2 a_1^2 m_1 + 2I_1 a_2^2 m_2 - L_1^2 a_2^2 m_2^2 \cos(2\phi_1 - 2\phi_2) + 2a_1^2 a_2^2 m_1 m_2) \end{aligned}$$

and

$$\begin{aligned} \ddot{\phi}_2 = & (a_2 m_2 (2I_1 g \sin(\phi_2) + 2L_1^3 \dot{\phi}_1^2 m_2 \sin(\phi_1 - \phi_2) + 2L_1^2 g m_2 \sin(\phi_2) + 2I_1 L_1 \dot{\phi}_1^2 \sin(\phi_1 - \phi_2) \\ & + 2a_1^2 g m_1 \sin(\phi_2) + L_1^2 a_2 \dot{\phi}_2^2 m_2 \sin(2\phi_1 - 2\phi_2) + 2L_1 a_1^2 \dot{\phi}_1^2 m_1 \sin(\phi_1 - \phi_2) \\ & - 2L_1^2 g m_2 \cos(\phi_1 - \phi_2) \sin(\phi_1) - 2L_1 a_1 g m_1 \cos(\phi_1 - \phi_2) \sin(\phi_1))) \\ & / (2(I_1 I_2 + L_1^2 a_2^2 m_2^2 + I_2 L_1^2 m_2 + I_2 a_1^2 m_1 + I_1 a_2^2 m_2 - L_1^2 a_2^2 m_2^2 \cos(\phi_1 - \phi_2)^2 + a_1^2 a_2^2 m_1 m_2)). \end{aligned}$$

If we use the values in Table. 3 we have

$$\begin{aligned} \ddot{\phi}_1 = & (-0.2808 \sin(2\phi_1 - 2\phi_2) \dot{\phi}_1^2 - 0.4136 \sin(\phi_1 - \phi_2) \dot{\phi}_2^2 \\ & + 10.3278 \sin(\phi_1 - 2\phi_2) + 38.2984 \sin(\phi_1)) / (1 - 0.2808 \cos(2\phi_1 - 2\phi_2)), \end{aligned}$$

and

$$\begin{aligned} \ddot{\phi}_2 = & (1.7390 \sin(\phi_1 - \phi_2) \dot{\phi}_1^2 + 0.2808 \sin(2\phi_1 - 2\phi_2) \dot{\phi}_2^2 \\ & - 33.02 \sin(2\phi_1 - \phi_2) + 30.9472 \sin(\phi_2)) / (1 - 0.2808 \cos(2\phi_1 - 2\phi_2)). \end{aligned}$$

With no noise, SINDy-PI discovers the correct equations. When we add random noise with magnitude of 0.005, SINDy-PI discovers the following

$$\begin{aligned} \ddot{\phi}_1 = & (-0.2799 \sin(2\phi_1 - 2\phi_2) \dot{\phi}_1^2 - 0.4137 \sin(\phi_1 - \phi_2) \dot{\phi}_2^2 + \\ & + 10.3429 \sin(\phi_1 - 2\phi_2) + 38.3117 \sin(\phi_1)) / (1 - 0.2815 \cos(2\phi_1 - 2\phi_2)), \end{aligned}$$

and

$$\begin{aligned} \ddot{\phi}_2 = & (1.7392 \sin(\phi_1 - \phi_2) \dot{\phi}_1^2 + 0.2805 \sin(2\phi_1 - 2\phi_2) \dot{\phi}_2^2 \\ & - 33.0035 \sin(2\phi_1 - \phi_2) + 30.9418 \sin(\phi_2)) / (1 - 0.2813 \cos(2\phi_1 - 2\phi_2)). \end{aligned}$$

If we increase the noise magnitude to 0.01 then the SINDy-PI discovered equation becomes

$$\begin{aligned}\ddot{\phi}_1 &= (-0.2768\dot{\phi}_1^2 \sin(2\phi_1 - 2\phi_2) - 0.4138 \sin(\phi_1 - \phi_2)\dot{\phi}_2^2 \\ &\quad + 10.3676 \sin(\phi_1 - 2\phi_2) + 38.3225 \sin(\phi_1))/(1 - 0.2818 \cos(2\phi_1 - 2\phi_2)),\end{aligned}$$

and

$$\begin{aligned}\ddot{\phi}_2 &= (1.7355 \sin(\phi_1 - \phi_2)\dot{\phi}_1^2 + 0.2794 \sin(2\phi_1 - 2\phi_2)\dot{\phi}_2^2 + 0.1675 \sin(2\phi_1 - 2\phi_2) \\ &\quad - 33.0445 \sin(2\phi_1 - \phi_2) + 31.0065 \sin(\phi_2))/(1 - 0.2819 \cos(2\phi_1 - 2\phi_2)).\end{aligned}$$

If we continue to increase the noise magnitude to 0.05 then SINDy-PI incorrectly identifies

$$\begin{aligned}\ddot{\phi}_1 &= (15.5413 \sin(\phi_1 - 2\phi_2) - 2.6396 \sin(\phi_1 - \phi_2) - 0.9538 \cos(\phi_1 - \phi_2) \\ &\quad + 35.9971 \cos(\phi_1 - 61/40) - 2.4160 \cos(\phi_2 - 1149/1000) - 0.0733 \cos(2\phi_1 - 2\phi_2) \\ &\quad + 0.0269 \cos(4\phi_1 - 2\phi_2) + 2.3419 \sin(2\phi_1 - \phi_2) + 0.5142\dot{\phi}_1 \sin(2\phi_1 - 2\phi_2) \\ &\quad - 0.4584\dot{\phi}_2 \sin(2\phi_1 - \phi_2) - 0.3807\dot{\phi}_2^2 \sin(\phi_1 - \phi_2) + 0.8810\dot{\phi}_1 \sin(\phi_1 - \phi_2) \\ &\quad + 0.9411\dot{\phi}_1 \sin(\phi_1 - 2\phi_2) - 0.7664\dot{\phi}_2 \sin(\phi_1 - \phi_2) + 1.2026)/(1 - 0.4245 \cos(2\phi_1 - 2\phi_2)),\end{aligned}$$

and

$$\ddot{\phi}_2 = 70.9 \sin(\phi_1 - \phi_2).$$

G SINDy-PI Model for the Belousov-Zhabotinsky Reaction

The SINDy-PI discovered PDE for the simplified BZ reaction is

$$\begin{aligned}x_\tau &= \Delta x + \frac{0.24667x + 0.33333s + 0.5z + 3.3333xs - 5.0xz + 2.1333x^2 - 3.3333x^3}{x + 0.1}, \\ z_\tau &= 0.01\Delta z + x + 0.4u - 1.3z, \\ s_\tau &= \Delta s + 0.17333r - 0.66667s, \\ u_\tau &= \Delta u - 133.33u + 100z.\end{aligned}$$

H Inability to Identify Rational Dynamics with SINDy

In this section, we demonstrate that it is not possible to identify rational dynamics with the original SINDy algorithm, testing it on the Michaelis-Menten dynamics in Eq. (18). We use the same parameters in Sec. 3.3. The Taylor expansion of Eq. (18) at $x = 0$ is

$$\dot{x} \approx 0.6 - 5x + \frac{50}{3}x^2 - \frac{500}{9}x^3 + \frac{5000}{27}x^4 - \frac{50000}{81}x^5. \quad (38)$$

Thus, when the trajectory provided for training is close enough to $x = 0$, SINDy should identify Eq. (38). To verify this, data with $x_0 = 0.2409$ is simulated for 22 time steps with $dt = 0.01$. Both the Implicit-SINDy and SINDy-PI algorithms identify the correct model in Eq. (18) with highly accurate parameters. The model identified by SINDy is

$$\dot{x} = 0.5914 - 4.7387x + 13.1389x^2 - 27.6470x^3 + 36.9846x^4 - 22.8388x^5. \quad (39)$$

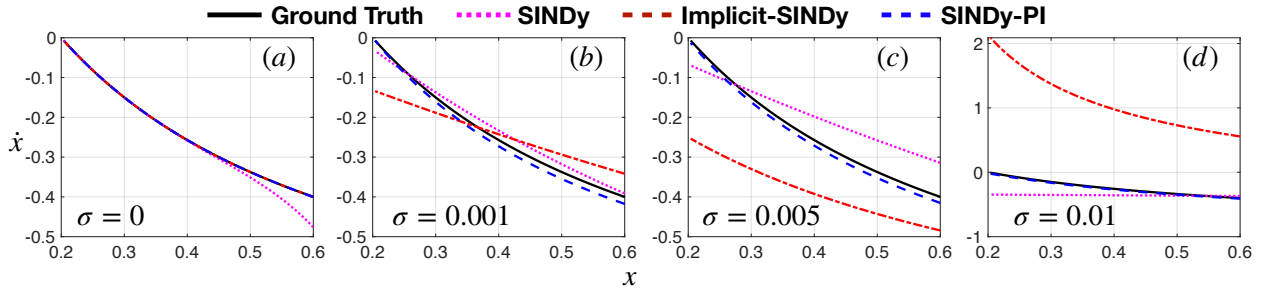


Figure 10: Comparison of the model identified by SINDy, Implicit-SINDy, and SINDy-PI on Michaelis-Menten dynamics.

Thus, SINDy correctly identifies the first three terms of the Taylor expansion, although the higher order terms have large parameter errors. This model is compared with the SINDy-PI and Implicit-SINDy models in Fig. 10 for a test trajectory initialized with $x_0 = 0.6$. From Fig. 10 (a), it can be seen that both SINDy-PI and Implicit-SINDy match the true solution. However, the SINDy model only agrees for x near the origin. When Gaussian noise of magnitude σ is added, the SINDy model degrades further. Moreover, the amount of data used needs to be increased to identify the correct model. In Fig. 10 (b) to (d), 330, 2200 and 4400 data points ranging from 0 to 12 are used for training. The same amount of data is used for model selection. From Fig. 10 (b) to (d), it can be seen that the SINDy model does not work well away from $x = 0$.

I Robustness of SINDy and SINDy-PI

The robustness of SINDy-PI to noise depends on a number of factors, including the length of the data, which initial conditions are chosen to generate the data, the model parameters, the order of the polynomial terms in the model, etc. The relative impact of all of these factors varies with the system we are studying.

In general, training data that explores more of the phase space will result in a more robust model discovery process. Generally speaking, data that results in a better-conditioned Θ matrix will provide more robust results. Several studies have explored strategies to improve the robustness, with Wu and Xiu suggesting the use of a large ensemble of initial conditions [43]. Exciting transients is also important [28].

Another key factor that affects the condition number of Θ is the number of library elements, which is determined by the order for a polynomial library. Including higher-order terms increases the condition number, making it more difficult to accurately disambiguate which nonlinear term is responsible for the observed behavior. The library size scales exponentially with the maximum polynomial order.

Noise robustness is also affected by the model parameters. Smaller parameters in Ξ are more likely to be removed during thresholding, making the procedure less robust to noise. To illustrate this, we change the parameter K_m in Eq. s4eq1 and test the maximum noise SINDy-PI can handle. We set K_m equal to 0.01, 0.1, 1 and 10 separately. We generate the training data with 120 random initial conditions ranging from 0 to 10. Each initial condition is simulated until $T = 5$ with $dt = 0.01$, and the same magnitude of Gaussian noise is added. TVRegDiff is used to calculate the derivative, and the first and last 30% percent of data is discarded due to aliasing effect. The testing data is generated using the same process and the ratio of training and testing data is 1 : 1. The model and maximum magnitude of noise allowed for each values of K_m is summarized in Table 8. These results suggest that as K_m increases, the maximum noise SINDy-PI can handle also increases.

Table 8: The effect of K_m on the noise robustness of SINDy-PI.

K_m	Max Magnitude of Noise	True Model	Identified Model
0.01	0.001	$\dot{x} = -\frac{(0.9x-0.006)}{x+0.01}$	$\dot{x} = -\frac{(x-7.6144)(x-5.6092)(x-2.5078)(x-0.0072)}{(x-7.6146)(x-5.6125)(x-2.5092)(x+0.0092)}$
0.1	0.01	$\dot{x} = -\frac{(0.9x-0.06)}{x+0.1}$	$\dot{x} = -\frac{(x-5.4132)(x-0.0681)}{(x-5.4144)(x+0.099)}$
1	0.05	$\dot{x} = -\frac{(0.9x-0.6)}{x+1}$	$\dot{x} = -\frac{(x-4.7143)(x-0.6726)}{(x-4.7159)(x+0.9698)}$
10	0.1	$\dot{x} = -\frac{(0.9x-6)}{x+10}$	$\dot{x} = -\frac{0.99x-6.583}{x+11.07}$